COO-1112-5

THE UNIVERSITY OF MICHIGAN
COLLEGE OF LITERATURE, SCIENCE, AND THE ARTS
Department of Physics

Technical Report

LAMBDA-PROTON INTERACTIONS

Walter L. Gibbs

ORA Project 04938

under contract with:

U. S. ATOMIC ENERGY COMMISSION
CHICAGO OPERATIONS OFFICE
CONTRACT NO. AT(11-1)-1112
ARGONNE, ILLINOIS

administered through:

OFFICE OF RESEARCH ADMINISTRATION ANN ARBOR

November 1967

This report was also a dissertation submitted in partial fulfillment of the requirements for the degree of Doctor of Philosophy in The University of Michigan, 1967.

TABLE OF CONTENTS

LIST OF FIGURES

ABSTRACT

LAMBDA-PROTON INTERACTIONS

By Walter L. Gibbs

This research was undertaken in order to study the lambda-proton interaction having a center of mass energy ranging between 2050 Mev and 3500 Mev, with particular attention being paid to the possibility of resonance phenomena. The experiment is part of a study of the interactions of 3.65 Bev/c π^+ mesons in a deuterium filled bubble chamber. The lambdas were created in reactions of the type $\pi^+ d \rightarrow p \Lambda (K\pi)^+$, where $(K\pi)^+$ is a combination of pions and kaons which have net positive charge, isospin 1/2 or 3/2, and srangeness + 1.

Departures in the behavior of protons and lambdas from the behavior predicted by assumming no interaction are carefully examined. The behavior of the proton is examined in light of the "spectator model", based on the "impulse approximation" and the Hulthén theory of the deuteron. The behavior of the lambda is examined in light of properties of the reaction $\pi^- p \rightarrow \Lambda (K\pi)^\circ$, where $(K\pi)^\circ$ is a combination of pions and kaons having strangeness +1, isospin 1/2 or 3/2, and zero net charge. This reaction is charge symmetric to the reaction $\pi^+ N \rightarrow \Lambda (K\pi)^+$ and, assuming charge symmetry, the cross sections are equal.

The Λ-P effective mass spectrum is especially interesting.

Although this spectrum, when contrasted to a background of non-interacting events, reaveals none of the previously announced resonances, there is a significant accumulation of events above background in the range 2100-2200 Mev. This enhancement, whose center is at 2125 Mev, and whose width at half maximum is 40 Mev is discussed in terms of Λ-P elastic scattering and phenomena associated with the Σ-N threshold at 2130 Mev.

CHAPTER 1

INTRODUCTION

1-1. Introductory Remarks

Unlike the two nucleon system, most of whose features have been amply studied over the last thirty-five years, the story of the lambda-nucleon system is just now beginning to unfold. A complete description of the lambda-nucleon system must include a knowledge of the scattering properties, the angular distribution and cross section as a function of energy, as well as a knowledge of the bound and non-bound, or resonance, states of the system. The possibilities of a bound state or a resonance in the lambda-nucleon system are of special interest. At present, the deuteron is the only known bound state between two baryons, and no baryon-baryon resonance has yet been conclusively established. On the basis of SU_3 symmetry predictions, nine "particles" may be placed in a $\overline{10}$ decuplet with the deuteron. All of these particles would have spin = 1, baryon number = 2, and they would include, besides the S(strangeness)= 0 deuteron, an S = 1 isospin doublet, an S = -2 triplet, and an S = -3 quartet. The S = -1 doublet would presumably be coupled via the strong interactions to ΛP and ΛN.

This experiment was undertaken to study the ΛP interaction having a center of mass energy ranging between 2050 Mev and 3500 Mev, with particular attention being

paid to the possibility of resonance phenomena. The experiment is part of a study of interactions of 3.65 BeV/C π^+ mesons in a deuterium filled bubble chamber. The lambdas were created in reactions of the type

$$\pi^+ \, d \rightarrow p \, \Lambda \, (K\pi)^+$$

where $(K\pi)^+$ is a combination of pions and kaons which have net positive charge, isospin 1/2 or 3/2, and strangeness + 1, that is

$$(K\pi)^+ = K^+ \, , \; K^+ \pi^\circ \, , \; K^\circ \pi^+ \, , \; K^+ \pi^+ \pi^- \, , \text{ etc.}$$

Only the final states of the lambda and proton are directly observable, so that any properties relating to the initial state must be inferred. It is presumed that the positive pion hits the neutron in the deuteron, creates a lambda, a kaon, and perhaps some additional pions, and then the lambda subsequently interacts with the proton. Certain ambiguities, however, are implicit in such an experiment. First, the initial momentum of the proton in the deuteron is not known, so that it is not always clear whether the lambda and proton have indeed interacted; the proton may act as a mere spectator to the reaction. Moreover, the final state contains a kaon, and perhaps pions as well, which may have interacted strongly with the proton, the lambda, or both, and there is, in general, no way to determine that the

sequence of reactions is as described above.

A more straightforward way to study the ΛN interaction is to observe scattering events directly. This can be accomplished by creating lambdas of known momentum in collisions of the type

$$\pi^- + P \rightarrow \Lambda + K^\circ$$

and then looking for scattering events involving the Λ, such as

$$\Lambda P \rightarrow \Lambda P$$

A number of experiments of this kind have been performed, the results of which will be discussed below. The chief advantage of a deuterium experiment over the direct approach is that the lambda is created in the immediate vicinity of the proton, and thus has ample opportunity to interact. This produces many more events than one could expect from a comparable experiment using the direct approach, because of the short Λ lifetime, so that resonance phenomena are possibly more readily examined.

1-2. Λ-P Elastic Scattering.

The first examples of Λ-P elastic scattering were observed in 1959 by Crawford et al.(1959) A sample of 650 Λ's from associated production:

$$\pi^- + P \rightarrow \Lambda + K^\circ$$

with momenta ranging from 500 to 1000 Mev/c yielded 4

elastic scattering events, from which an average cross section of 40 ± 20 mb was calculated.

Since then, a number of similar experiments have been performed, and in lieu of describing them chronologically we will summarize their results grouped according to momentum range.

Low momentum: $P_\Lambda \lesssim 400$ Mev.

The experiments of Alexander et al (1965), Sechi-Zorn et al (1964) and Pieckenbrock et al (1964) yielded a total of 314 elastic scattering events with Λ momentum ranging from 120 Mev/c to 400 Mev/c. The results, shown in Figure 1, are seen to be not entirely in agreement with one another. It is clear from this figure, however, that the cross section rises rapidly as momentum decreases, typical of many other elastic scattering cross sections. This rapid rise at low momentum seems to be adequately described by the effective range approximation:

$$\sigma = \frac{3\pi}{k^2 + [1/a_t - 1/2\, r_t\, k^2]^2} + \frac{\pi}{k^2 + [1/a_s - 1/2\, r_s\, k^2]^2}$$

where k is the lambda wave number and a_t, r_t, a_s and r_s are adjustable parameters of the theory. Alexander et al (1965) found values of

$$a_s = -2.46 \text{ f} \qquad a_t = -2.07 \text{ f}$$
$$r_s = 3.87 \text{ f} \qquad r_t = 4.5 \text{ f}$$

whereas Sechi-Zorn et al (1964) found

$$a_s = -3.6 \text{ f} \qquad r_s = 2 \text{ f}$$
$$a_t = -5.3 \text{ f} \qquad r_t = 5 \text{ f}$$

Other forms beside the effective range formula above also describe the rapid rise of the cross section at low momentum shown in Figure 1. Ali et al (1956) has fit cross sections calculated from simple potential models (in the Born approximation) and found that the low energy data was best described (in a least squares sense) by a Yukawa potential

$$V = -U \, (\mu^3/4\pi) \exp(-\mu r)/\mu r$$

with

$$\mu = 1.024 \text{ f}^{-1}$$
$$U = 454 \text{ MeV f}^3$$

A complete study of the angular distribution is difficult to perform in the low energy region due to the fact that small angle scatters yield a proton which does not go far enough in the bubble chamber to be detected. Alexander et al (1965) finds that the angular distribution of visible events is roughly isotropic. Sechi-Zorn (1965), however, finds a forward peaking in the angular distribution above P = 260 Mev/c as does Piekenbrock.

Intermediate momentum: $400 \lesssim P \lesssim 1500$ Mev/c.

Roughly 200 ΛP elastic scattering events have been observed in the region $400 \lesssim P \lesssim 1500$ Mev/c by a number

of researchers: Alexander et al (1961), Arbuzov et al (1962), Groves (1963), Beilliere (1964) and Cline et al (1967). The results are plotted in Figure 2, and are consistent with a constant cross section in this momentum region.

Taken in toto, the angular distribution in this region is consistent with isotropy, although Arbuzov (1962) sees an angular distribution peaked in the backward direction, and Groves (1963) sees a distribution peaked slightly forward.

High momentum: P > 1000 Mev/c

Seventy high momentum events have been recorded by Vishnevskii et al (1966) and Bassano et al (1967). The cross sections are plotted in Figure 2. As Bassano et al (1967) points out, the slow decrease of the ΛP cross section at high energy is similar to the well known behavior of the PP elastic cross section and moreover, the two total cross sections are virtually identical in magnitude at high energy. The angular distribution is strongly peaked in the forward direction at high energy just as is the PP angular distribution.

In toto, the elastic scattering data is too meager to reveal a resonance in the Λ-P system unless its width is extremely broad.

1-3. Outline of the report

The scheme of this report is as follows. In

Chapter 2 we discuss the genesis of the events studied and the reduction of the data relevant to the experiment. Chapter 3 deals with the presence of the two body meson-baryon and meson-meson resonances in our data and how they are detected, and Chapter 4 examines our findings with respect to the ΛP interaction and presents our conclusions.

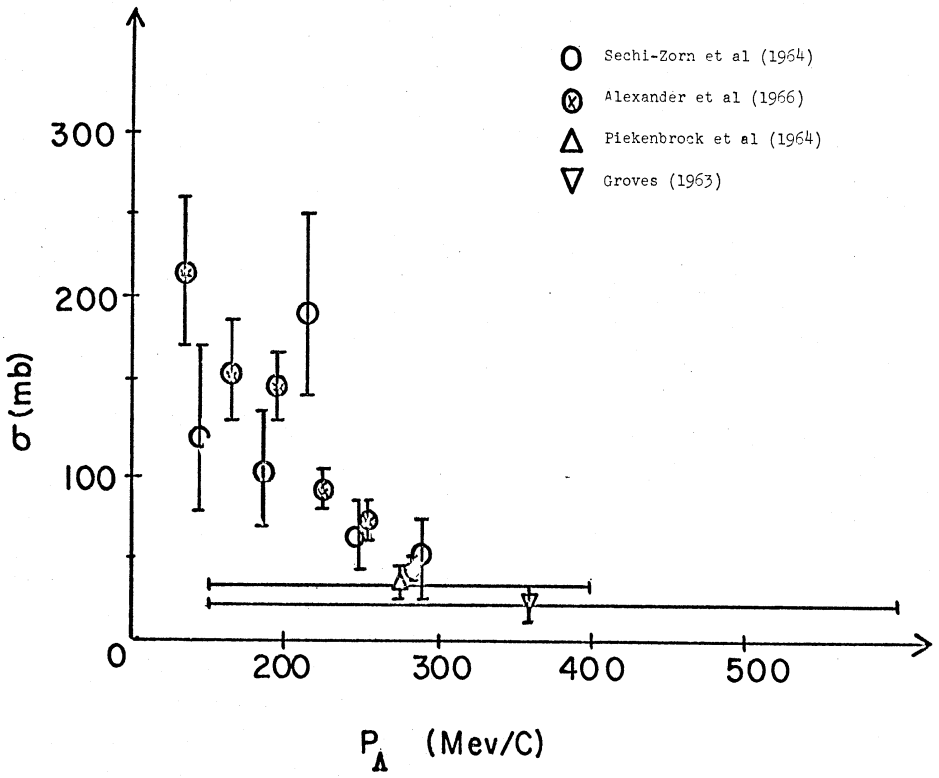

Fig 1. The low energy Λ-P elastic scattering data.

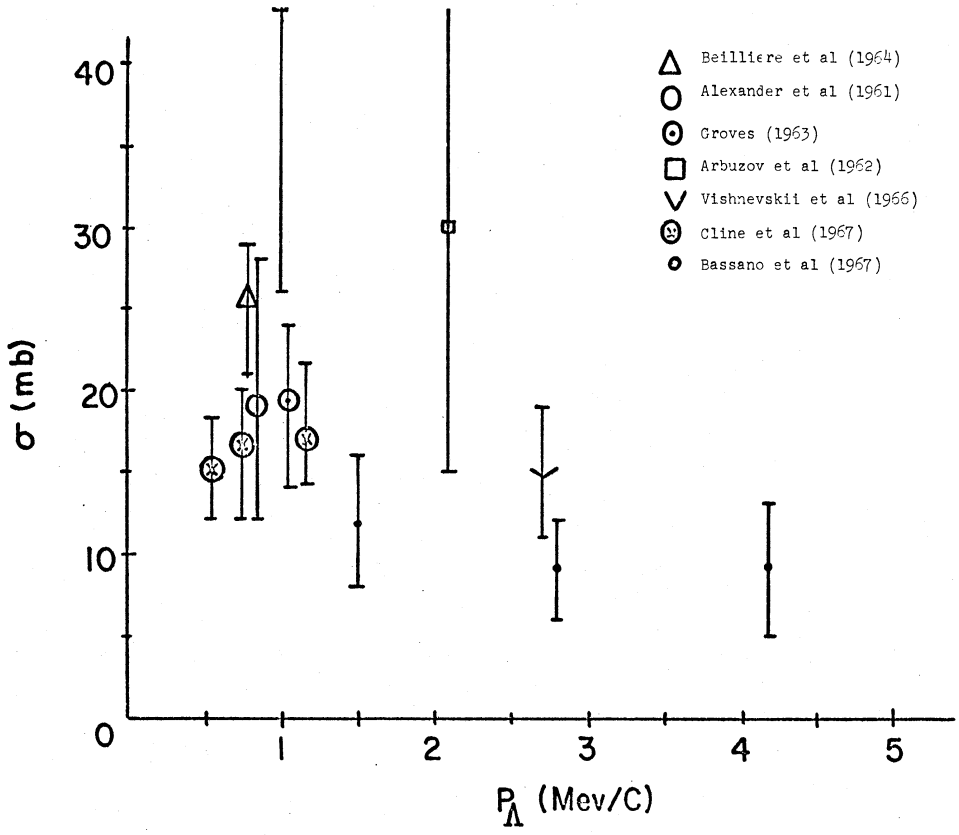

Fig 2. The intermediate and high energy Λ-P elastic scattering data.

CHAPTER 2

THE DATA AND ITS REDUCTION

2-1. Reduction of Data

The film analyzed in this experiment was exposed in the Brookhaven 20-inch deuterium chamber in 1963-64. The total exposure produced 256,500 frames, of roughly 15 beam tracks per picture. The pictures were then scanned and measured at Randall Laboratory, using the four scanning machines and three measuring machines available. A description of these machines may be found in Moebs (1965). Both scanning and measuring machines project the film onto a green translucent screen and magnify the image. The scanning machines magnify the image to 1.3 times life-size on three machines and 1.1 times life-size on the other. All the events were measured at a magnification of 2.6 times life-size.

The events studied in this report were distinguished by having a lambda coming from an interaction vertex with a slow proton. Acceptable events may have one V, such as in the reaction

$$\pi+ \; D \rightarrow K+ \; P \; \Lambda$$

or two V's, as in the reaction

$$\pi+ \; D \rightarrow \pi+ \; P \; \Lambda \; K^{\circ}$$

Moreover, the interaction vertex may have additional $\pi+ \; \pi^-$ pairs, so that four or even six prong events with one or two V's were found. Examples of the major types of topologies found are shown in Figures 3 - 6.

The scanning procedure used to locate events with a possible lambda-proton final state interaction

was as follows. Each frame was first scanned for V's. Once a V was found, the positive prong was checked with a template relating curvature and bubble density for protons and π+'s. If this simple check showed the positive prong was consistent with being a proton, and hence the V was consistent with being a lambda, a vertex was looked for which satisfied the criterion that the line joining the vertex and the tip of the V split the prongs of the V. Next, each positive prong of the vertex was examined to see if it was consistent with being a proton. Positive tracks which stopped without decaying yielded the best proton candidates. In the case where no such stopping track was available, each non-decaying positive prong of the vertex was examined with the curvature - bubble density template. If it was possible to associate more than one vertex with a proton candidate with a particular lambda, an expecially constructed template was used to help resolve the ambiguity. This template compared the angle the proton from the lambda decay makes with the flight path of the lambda, and the bubble density of that proton predictded by a Lorentz transformation from the rest frame of the lambda, where the proton has a momentum consistent with

$$\vec{P}_{\pi}^{\,*} + -\vec{P}_{p}^{\,*} = \vec{P}^{*}$$

$$\sqrt{P^{*2} + M_{\pi}^{2}} + \sqrt{P^{*2} + M_{p}^{2}} - M_{\pi} - M_{p} = 37 \text{ Mev}$$

That is, the magnitude of the proton momentum in the lambda rest frame is determined uniquely; it must be equal to 100 Mev/c:

$$\left|\vec{P}_{p}^{\,*}\right| = 100 \text{ Mev/c}$$

Since the component of the momentum transverse to the direction of the Lorentz transformation is unchanged by that transformation, i.e.,

$$\left|\vec{P}_{L}\right| \sin \theta_{L} = P^{*} \sin \theta^{*}$$

the laboratory momentum of the proton must obey the inequality:

$$\left|\vec{P}_{L}\right| \leq P^{*}/\sin \theta_{L}$$

This relationship places a lower bound on the bubble density of a proton making an angle less than a specified angle with the flight path, since the bubble density is related to the laboratory momentum as follows:

$$\text{bubble density} \sim 1 + (M/P_{L})^{2}$$

where M is the mass of the particle.

If an ambiguity still remained as to which vertex was to be associated with a particular V, both vertices were measured, and one vertex subsequently eliminated by a coplanarity test to be described below.

If a vertex was found to have a positive prong consistent with being a proton, the following information was recorded by the scanners: The frame number of the event the bubble density of the vertex proton (or, in the case of a stopping proton, its length), the bubble density or the length of the lambda proton, the number and nature of the other prongs of the vertex, and finally, whether another V particle was present.

A single scan of the film produced 2,579 events recorded in this manner. Part of the film was scanned independently, yielding an estimated scan efficiency of 70%.

The coordinates of the tracks in both the vertex and the V were recorded on one of the Michigan digitizers * and the results were run through the computer programs CHECK, which makes sure the measurement conforms to the proper format, and TRED, which fits a second order curve to the measured points, and thus reconstructs the track in three-dimensional space. TRED then computes the components of the momentum, the momentum errors, and the bubble density of each track for five different mass hypotheses (electron, π , K , proton, deuteron). The coordinates of the vertex and the

* For a description of these machines, see Moebs (1965).

tip of the V are also available in TRED, so that the flight path of the lambda is readily calculable from TRED output.

TRED was not always successful in reconstructing tracks in three-dimensional space, however, due to faultily measured points or awkward camera perspectives. Three-hundred and one events failed TRED twice and we eliminated them from the sample.

The 2,278 events which had successfully passed through TRED were then run through a single program which calculated the effective mass of the lambda and the coplanarity angle, i.e., the angle between the flight path of the lambda and the normal to its decay plane. Only those 1,141 events whose lambda effective mass lay within the interval $1100 < M_{\Lambda} < 1130$, and whose cosine of the coplanarity angle lay within the interval $-.08 < \cos 0 < .08$ were selected for further study.

Figures 7 and 8 show a plot of the coplanarity angle and lambda mass for the events which passed TRED. The width at half maximum of the coplanarity plot is about 2° , and the plot is consistent with symmetry about a coplararity angle of 90°. The width at half maximum in the lambda mass plot is about 6 Mev. The plot centers at the lambda mass of 1115 as expected,

and has a width consistent with being due entirely to our measurement errors.

Bubble density predictions of TRED were then compared with the observed bubble density to determine whether the protons in both V and the vertex were indeed protons. 540 events were eliminated in this manner, so that there were 601 events remaining which had a definite lambda associated with a vertex in which a proton resided.

2-2. Scan Biases

Both protons and lambdas are subject to consistent scan biases. The most serious bias is against slow protons which may stop before leaving a recognizable track in the chamber. No protons were observed with momenta less than 50 Mev/c, although on the basis of the impulse approximation, to be discussed below, a momentum of about 45 Mev/c should predominate. As shown in Figure 9, a proton with momenta less than 50 Mev/c travels a distance of less than .06 cm in the chamber, which, even under a magnification of 1.3 is too short to be observed. Protons with momenta in the range 50 to 100 Mev/c, traveling a distance of .06 to .6 cm in the chamber can be observed, but not consistently so. It was found, however, that those with momentum above 100 Mev/c, i.e., traveling a dis-

tance greater than .6 cm, were consistently found, and were consistent with the spectator model described below, in the region 100 Mev/c to 200 Mev/c. The bias against slow protons is not believed to be crucial for the study of Λ-P final state interactions since slow protons are deemed the least likely to have undergone interactions. This point will be discussed more fully subsequently.

Figure 10 shows the approximate dependence of bubble density on momentum for π's , K's and protons. It can be seen that fast protons are indistinguishable from π and K meson by means of bubble density analysis. The highest momentum at which a reasonably reliable distinction can be made is $\sim$ 1700 Mev/c, thus no proton with momentum greater than 1700 Mev/c was accepted, introducing a bias against fast protons. Although fast protons are believed to be among thos which have vigorously participated in interactions, relatively few protons have momenta greater than 1700 Mev/c.

A more serious form of bias results from lambdas

which decay so close to the vertex that they are indistinguishable from ordinary four or six prong events. Figure 11 shows the distribution of lambda laboratory path lengths. Although path lengths as short as .154 cm were observed, those lambdas with path lengths shorter than .2 cm were not found consistently. We may estimate the number of events lost in this manner by computing the distribution of the lifetimes in the rest frame of the Λ, and comparing the distribution with the theoretical distribution $e^{-t / \tau}$, where τ is the mean lifetime of the Λ. This is done in Figure 12, where the lifetime of the Λ in its rest frame has been calculated from the formula

$$\tau_\Lambda = MD / PC$$

where M is the mass of the Λ, and P and D its laboratory momentum and path length. The mean life used in Figure 12 is $2.61 \ 10^{-10}$ sec., which is the average of several published values.* The straight line fitted to the data on a semilog scale determines a Λ lifetime of $2 \pm .4 \ 10^{-10}$ sec. for this experiment, well within the range of the previously published values.

* The published values are found in Rosenfeld (1967).

Figure 12 shows that, although the curve remains exponential down to $t/\tau = .1$, there are about 60 events missing in the range $0 < t/\tau < .1$. These stem from lambdas which decay close to the interaction vertex and are confused with the prongs of the vertex.

In an effort to determine if these missing events introduce a serious bias into our lambda momentum spectrum we have calculated a corrected momentum spectrum as follows. We assume the probability of observing a lambda which has travelled a distance D in the laboratory is

$$Pr = e^{-\overline{D}/D}$$

where

$$\overline{D} = .2 \text{ cm}$$

By the above relation for the lifetime we may write this probability as a function of momentum:

$$Pr = e^{\frac{-\overline{D}\, M_\Lambda}{\tau_\Lambda \, PC}}$$

and thus obtain a relation between the number of observed events in a momentum interval N_o (P) and the actual number of events in that momentum interval N (P):

$$N\ (P) = N_o\ (P)\ /\ Pr$$

Figure 13 shows such a corrected lambda momentum spectrum with the number of events found by the above formula rounded off to the nearest integer. Although the weighting favors slower Λ's, since there were few slow Λ's observed experimentally, the missing events are more or less evenly distributed over the momentum range.

2-3 The Impulse Approximation and Spectator Protons

A 'spectator proton' we define as one which has not participated in any collision with another particle. The behavior of a spectator proton is predicted by the impulse approximation model.* In its simplest form, this model makes a two-fold prediction: In collisions between particles and deuterons, only one of the deuteron constituents is struck, and the nucleon which is not struck preserves the motion which it had at the moment of the collision.

The impulse approximation is based on three assumptions:

1. The projectile "sees" only one of the constituents of the deuteron.

* A description of this model in the context of the S matrix formalism may be found in G. F. Chew (1952).

The validity of this assumption depends on the energy of the projectile. Low energy projectiles are capable of discerning only the coarsest structure of the target since the de Broglie wavelength of the projectile, $\hbar/p$, is large. The Hulthén deuteron, as seen by a pion of 3.65 Bev/c, is depicted schematically in Figure 35 of appendix I. This picture shows an average distance between the nucleon centers of 3 fermis, while the individual nucleons have a radius of 1 fermi. This is an effective radius, taking the spatial extent of the pion at 3.65 Bev/c momentum into account. At our momentum, this assumption is justified to the extent that one can believe phenomenological theories of the deuteron.*

2. The collision is "sudden" in the sense that the collision time is small compared with the period of the deuteron. It R is the range of the force involved, and V the velocity of the projectile, the collision time is R/v. For pions at our momentum, this is roughly

$$t_c \approx 5 \times 10^{-24} \text{ sec.}$$

As shown in appendix I, the period of the deuteron is roughly 3.10^{-22} sec. so

* For a complete discussion of the deuteron see L. Hulthén (1957).

$$t_c / \tau \text{ deuteron} \approx 5/3\ 10^{-2} \ll 1$$

3. The deuteron is weakly bound in the sense that the binding energy is small compared with the collision energy. Since the pion nucleon center of mass energy is roughly 2800 Mev and the binding energy is 2.226 Mev, this criterion is amply fulfilled.

Thus, the assumptions of the impulse model are satisfied, and we might expect the proton momentum spectrum and angular distribution to be identical with those distributions prior to the collision. Since the deuteron is primarily S wave, (see Hulthén (1957)) and also unpolarized, there is no preferred direction in the lab. and the angular distribution should be isotropic. The momentum spectrum of the proton, as predicted by the Hulthén theory is given in Appendix I, Figure 36.

In Figures 14 and 15 we examine the proton distributions in light of the impulse model. Figure 14 shows the proton momentum distribution superimposed upon which is a Hulthén distribution normalized so that the areas under the two curves between 100 and 150 Mev/c agree. We see that discrepancies between the two curves start arising at 225 Mev/c and the faster protons are not described at all by the impulse model. Figure 15 shows the angular distribution of the protons made with respect

to the beam. The distribution in no way resembles the isotropic distribution predicted by the impulse model. Figure 16 shows the angular distribution between the proton and the lambda. It shows the proton and lambda tend to favor the same direction of motion.

2-4. The Strange Particles

No simple model, such as the impulse model, predicting the behavior of Λ's exists. Figure 17 shows the cosine of the angle the Λ makes with the beam. As one would expect, it is sharply canted in the forward direction. In Figure 18 we examine the laboratory momentum spectrum of the Λ. For comparison, we have included the lab momentum spectrum of Wangler (1966) from the reaction

$$\pi^- P \rightarrow \Lambda (K\pi)^\circ$$

at 2550 Mev.

This reaction is charge symmetric to the reaction

$$\pi^+ N \rightarrow \Lambda (K\pi)^+$$

and, assuming charge symmetry, the cross sections are equal. Since the πN center of mass energy is not a constant, but ranges from 2600 to 3100 Mev with an average value of 2750 Mev, we must, in addition, make the assumption that the momentum spectra are slowly

varying functions of the center of mass energy. Figure 18 shows our Λ's to be somewhat slower than those from π^- P, in spite of the higher average center of mass energy. This may be evidence for a Λ spectator proton secondary interaction. We will discuss this point in some detail in Chapter 4.

Figure 19 contrasts the K meson momentum spectra from the two experiments. They are very similar, except, as one would expect, the π^- P events are somewhat slower. Finally, Figure 20 depicts the 4 momentum transfer from the deuteron target to the Λ-P system. It is clear from the graph that low momentum transfer events predominate.

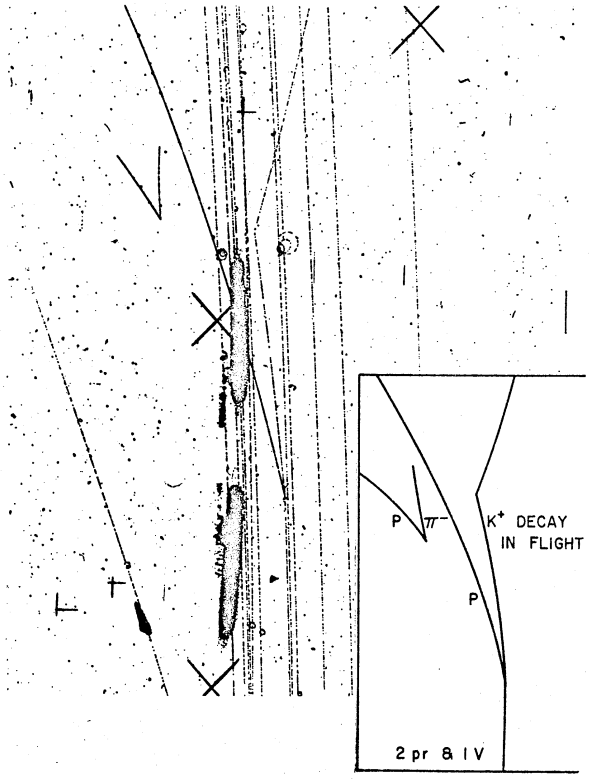

Fig 3. An example of event topology type 2 pr and 1 V.

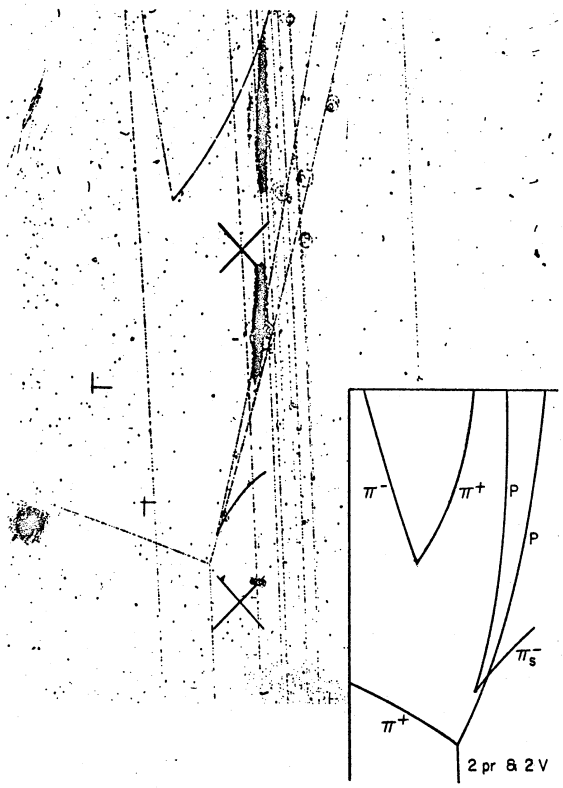

Fig 4. An example of event topology type 2 pr and 2 V's.

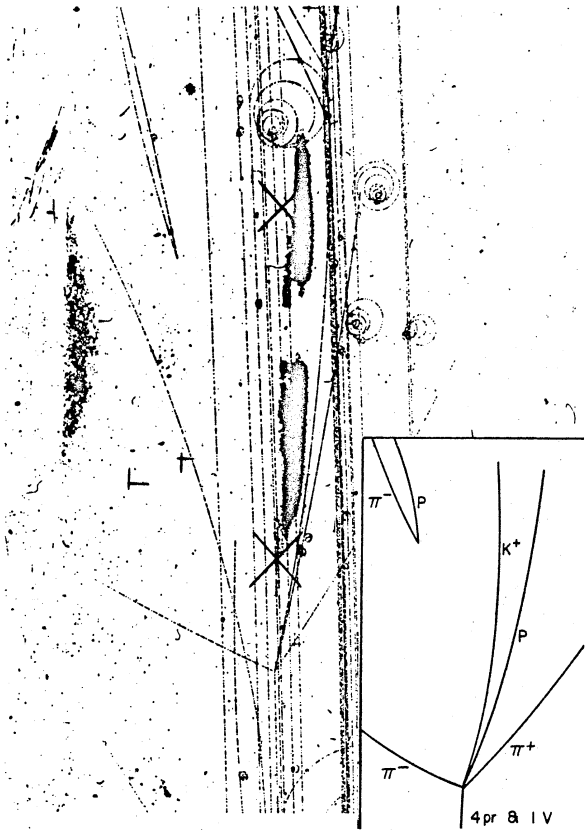

Fig 5. An example of event topology type 4 pr and 1 V.

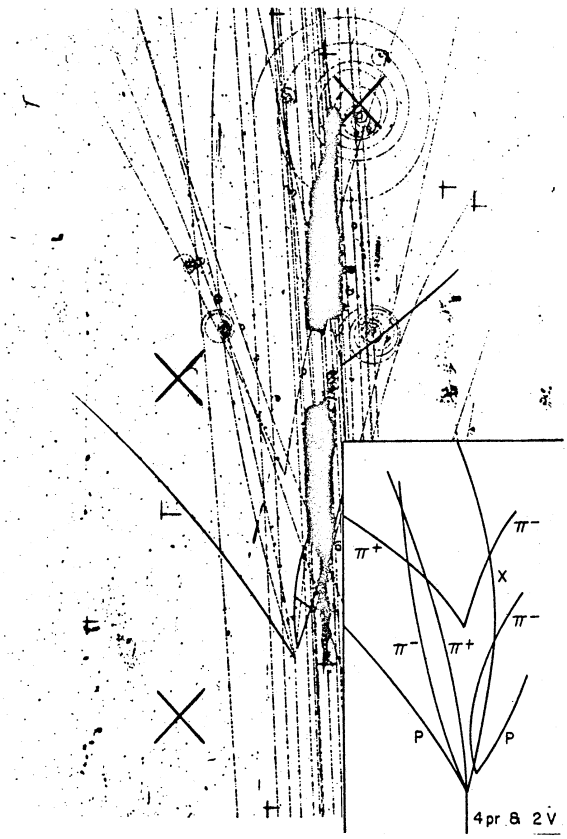

Fig 6. An example of event topology type 4 pr and 2 V's.

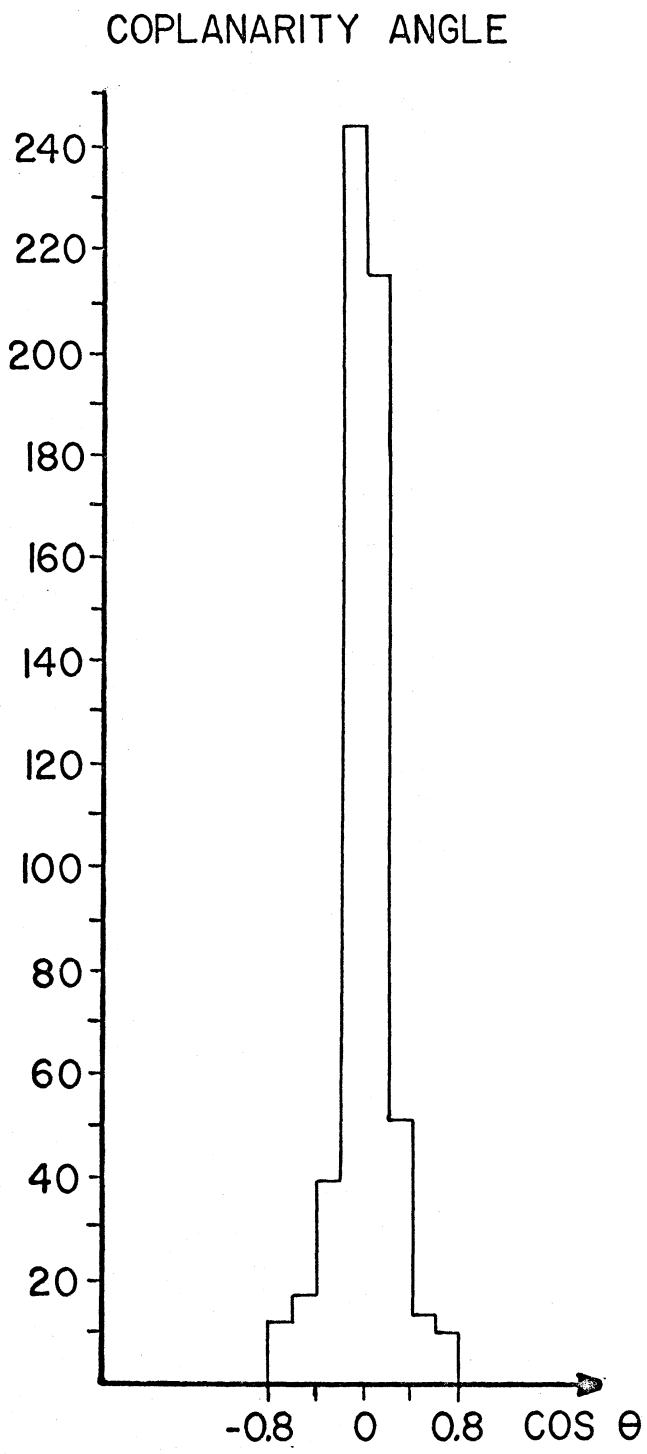

Fig 7. The coplanarity angle of the lambda. For a definition of this angle, see text.

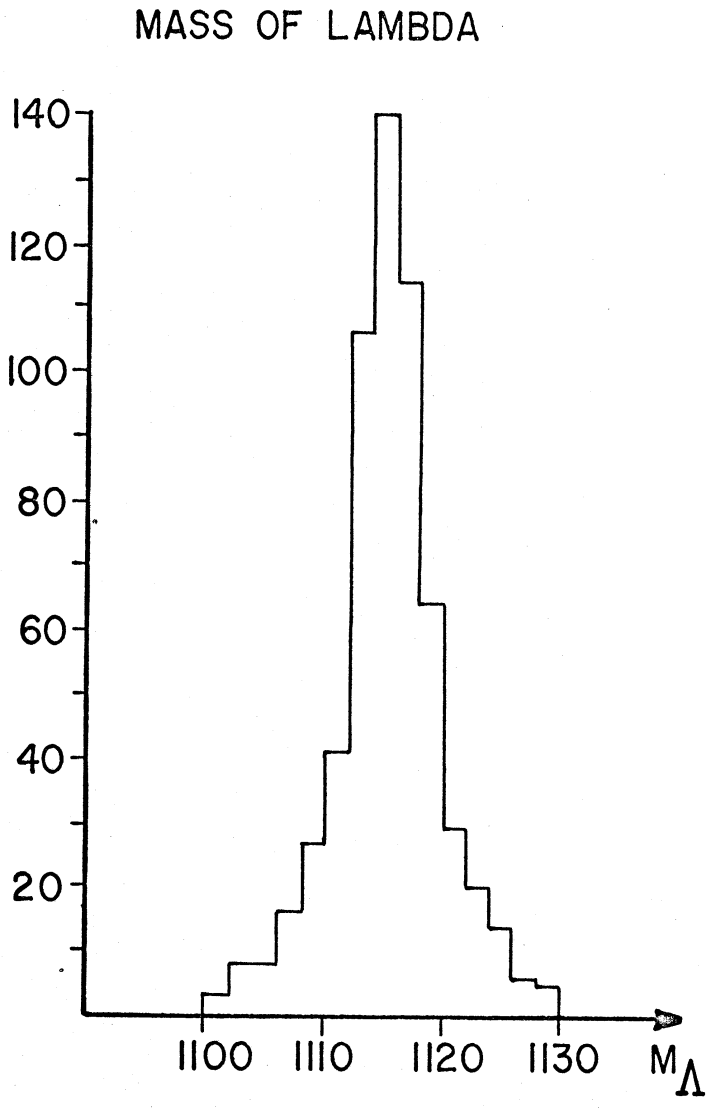

Fig 8. The mass of the lambda. The mass is centered at 1115. Mev and the width at half maximum is 6 Mev.

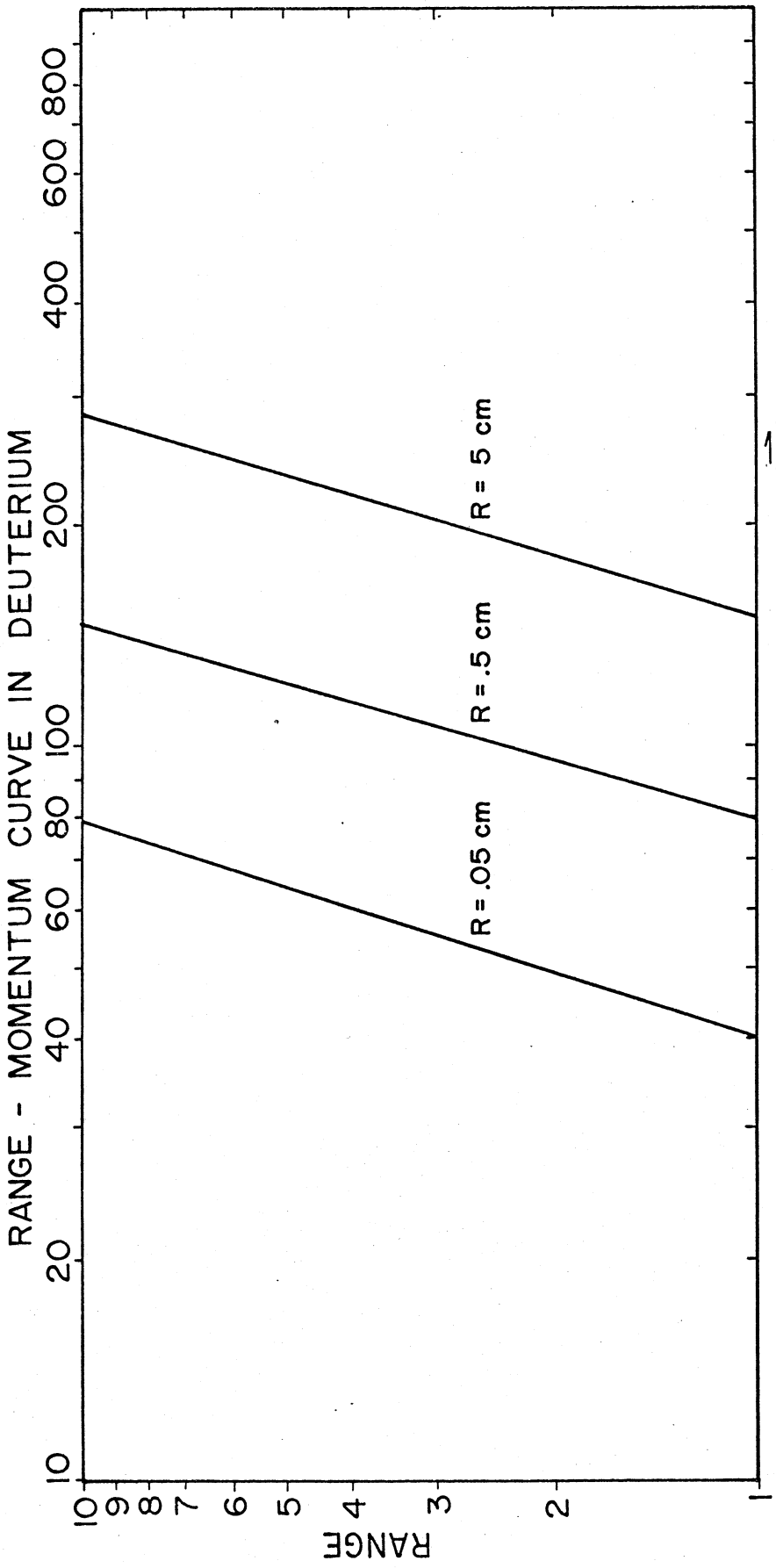

Fig 9. The range-momentum curve in deuterium.

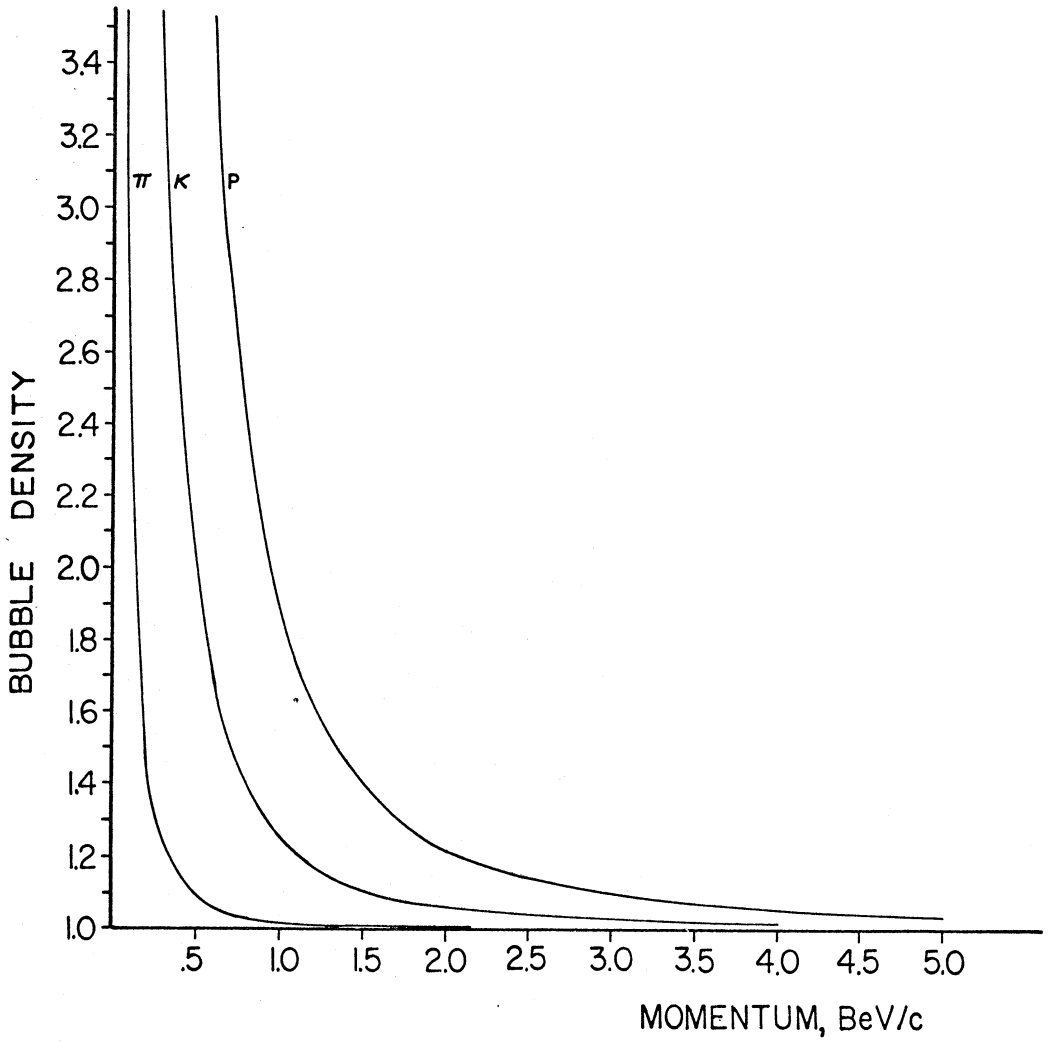

Fig 10. Bubble density vs particle momentum in deuterium.

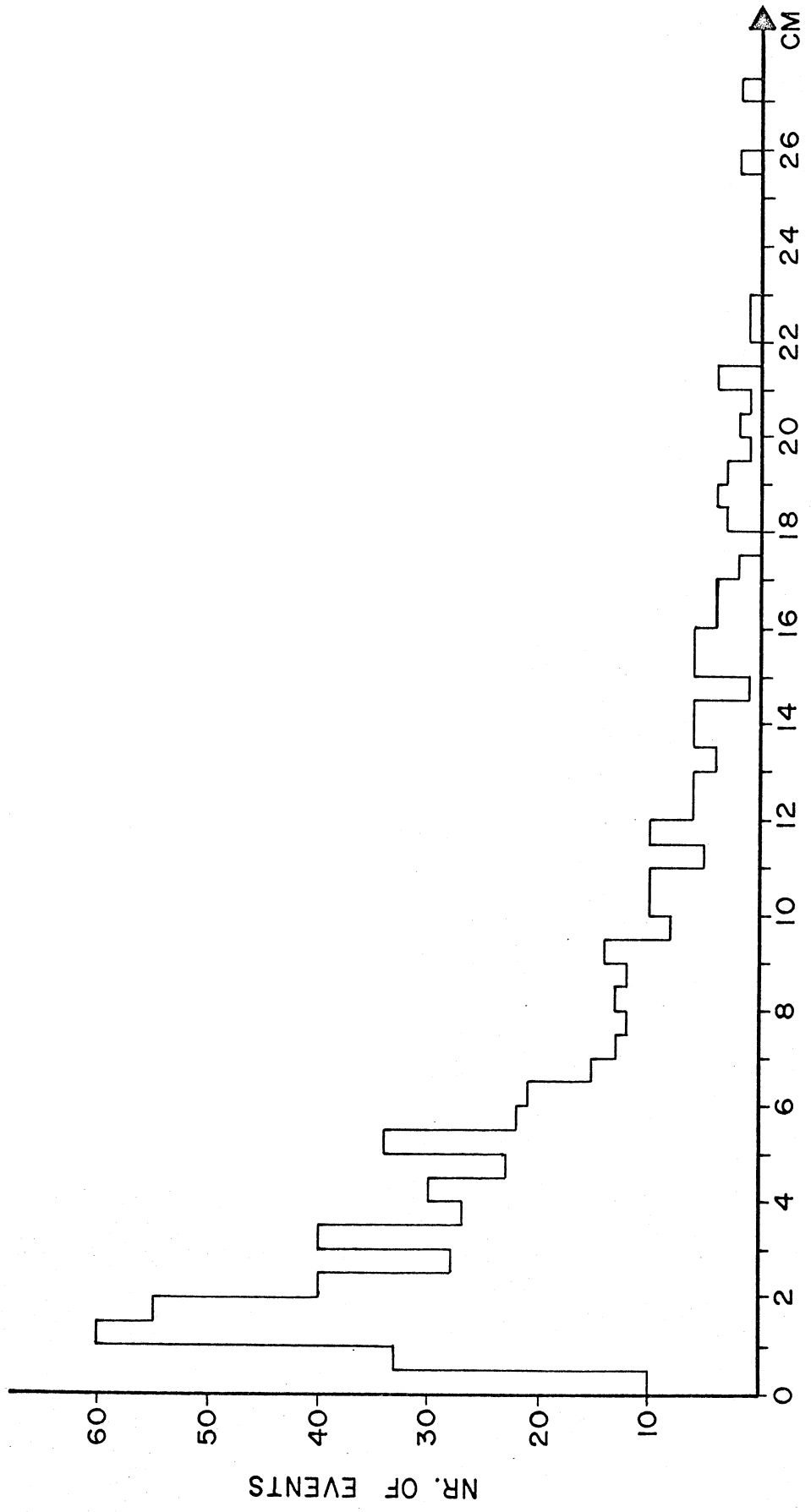

Fig 11. The lambda laboratory path length.

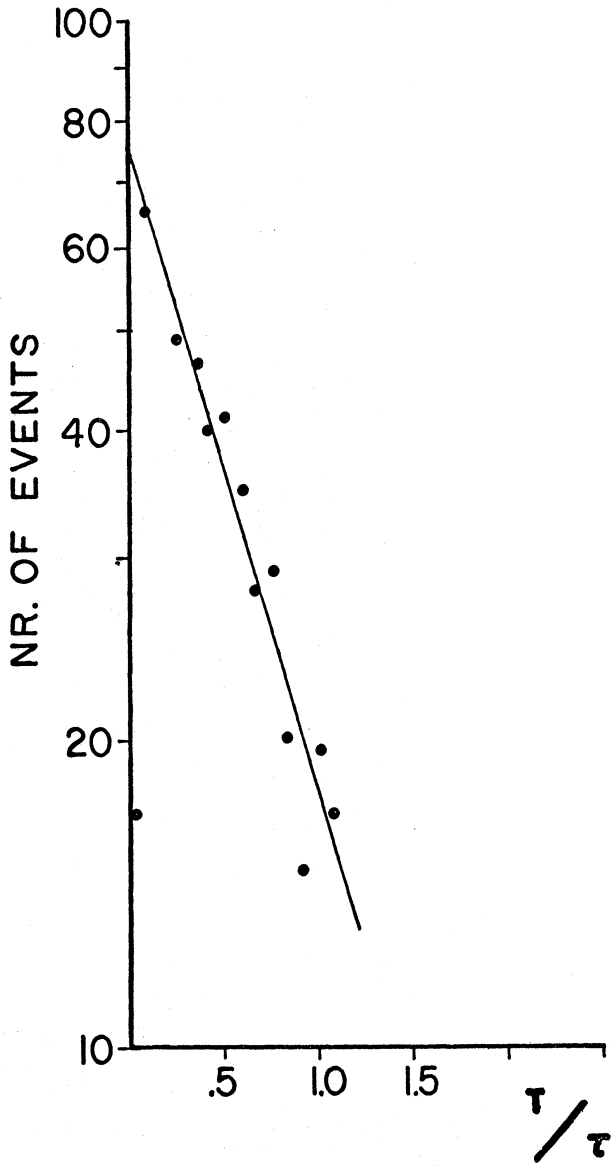

Fig 12. The life time of the lambda in its rest frame. τ is the average of several published values (See Text).

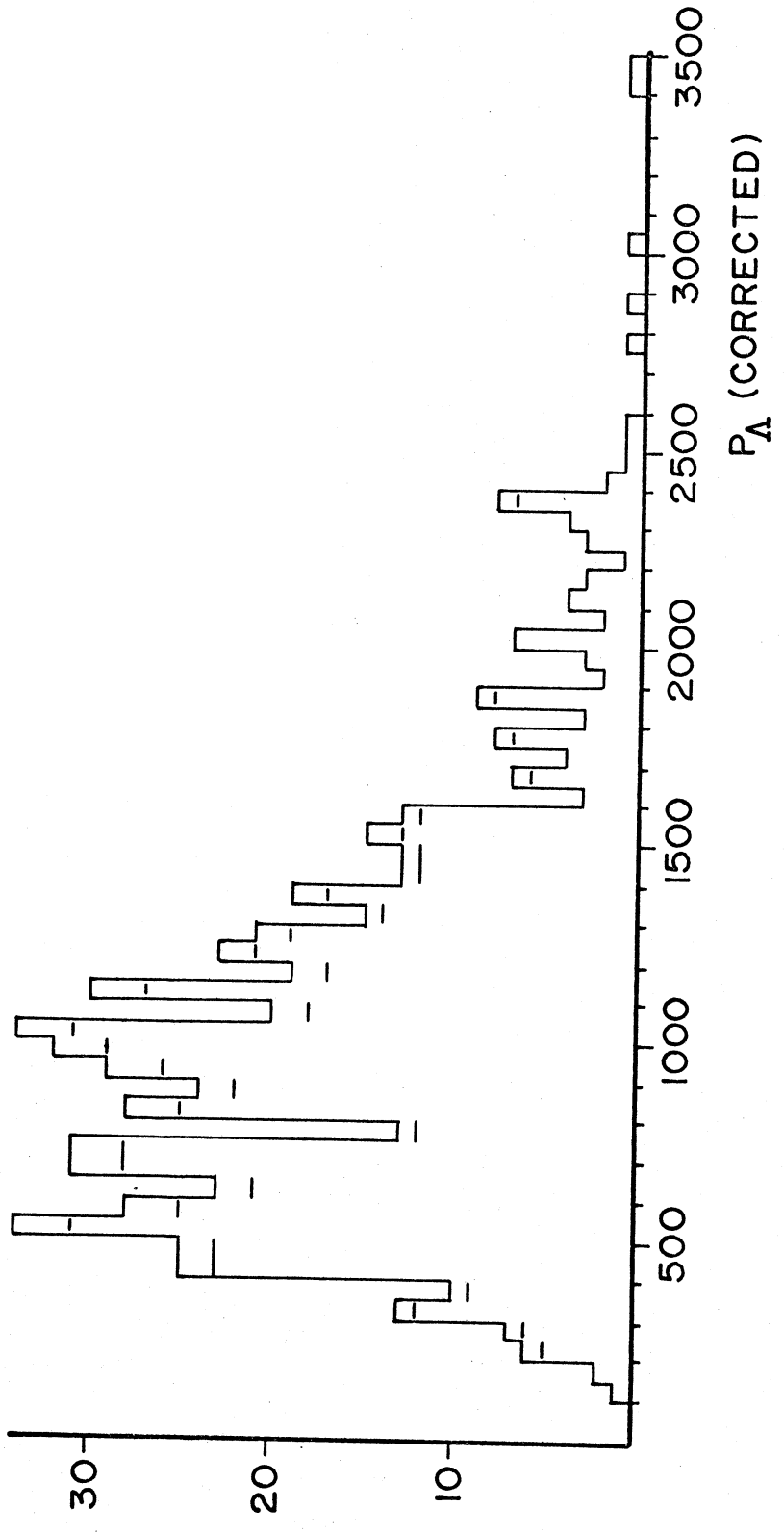

Fig 13. The lambda laboratory momentum spectrum corrected for the indetectibility of short traveling events. (see Text)

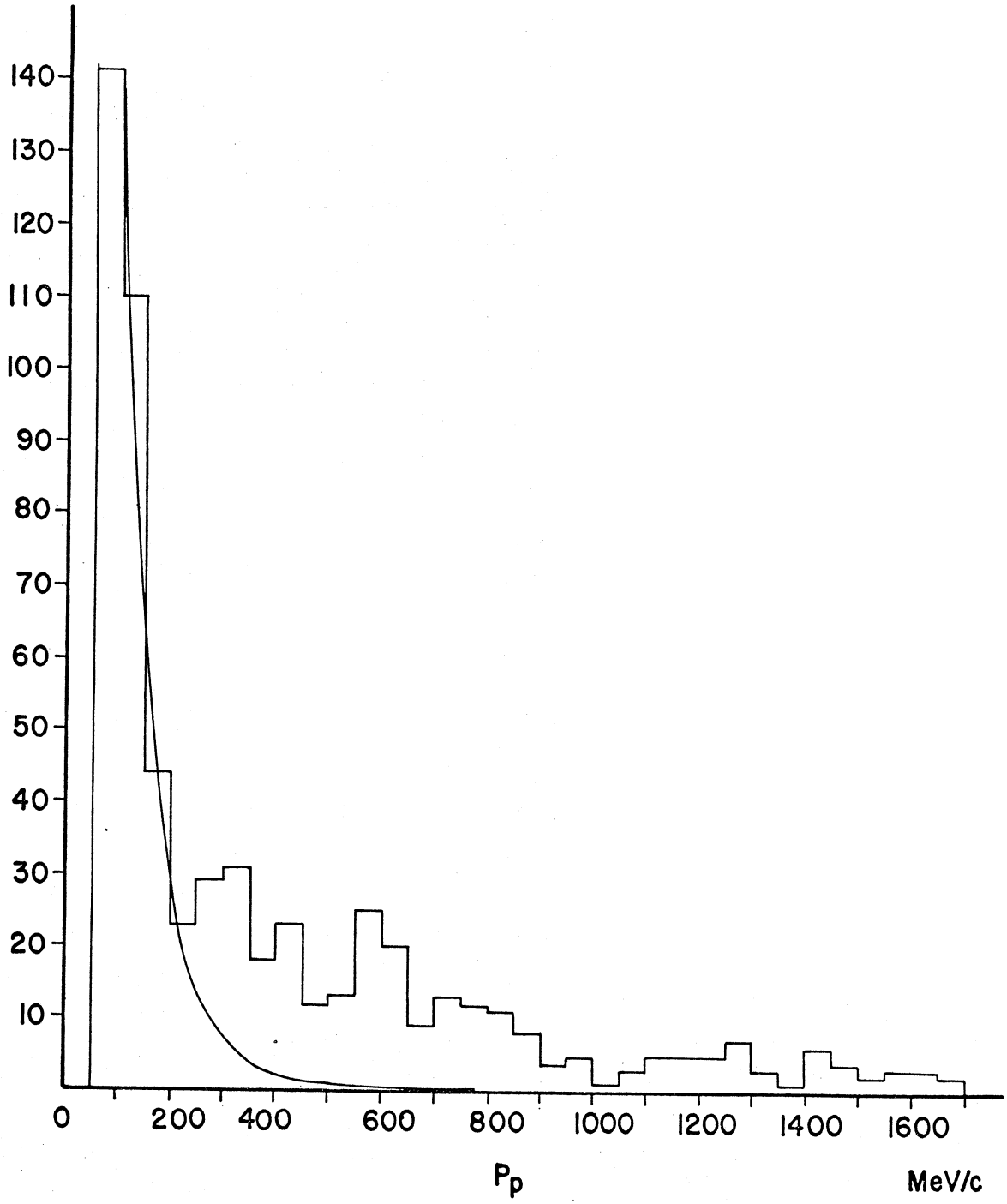

Fig 14. The laboratory proton momentum distribution. The smooth curve is the prediction of the spectator model. (See Text)

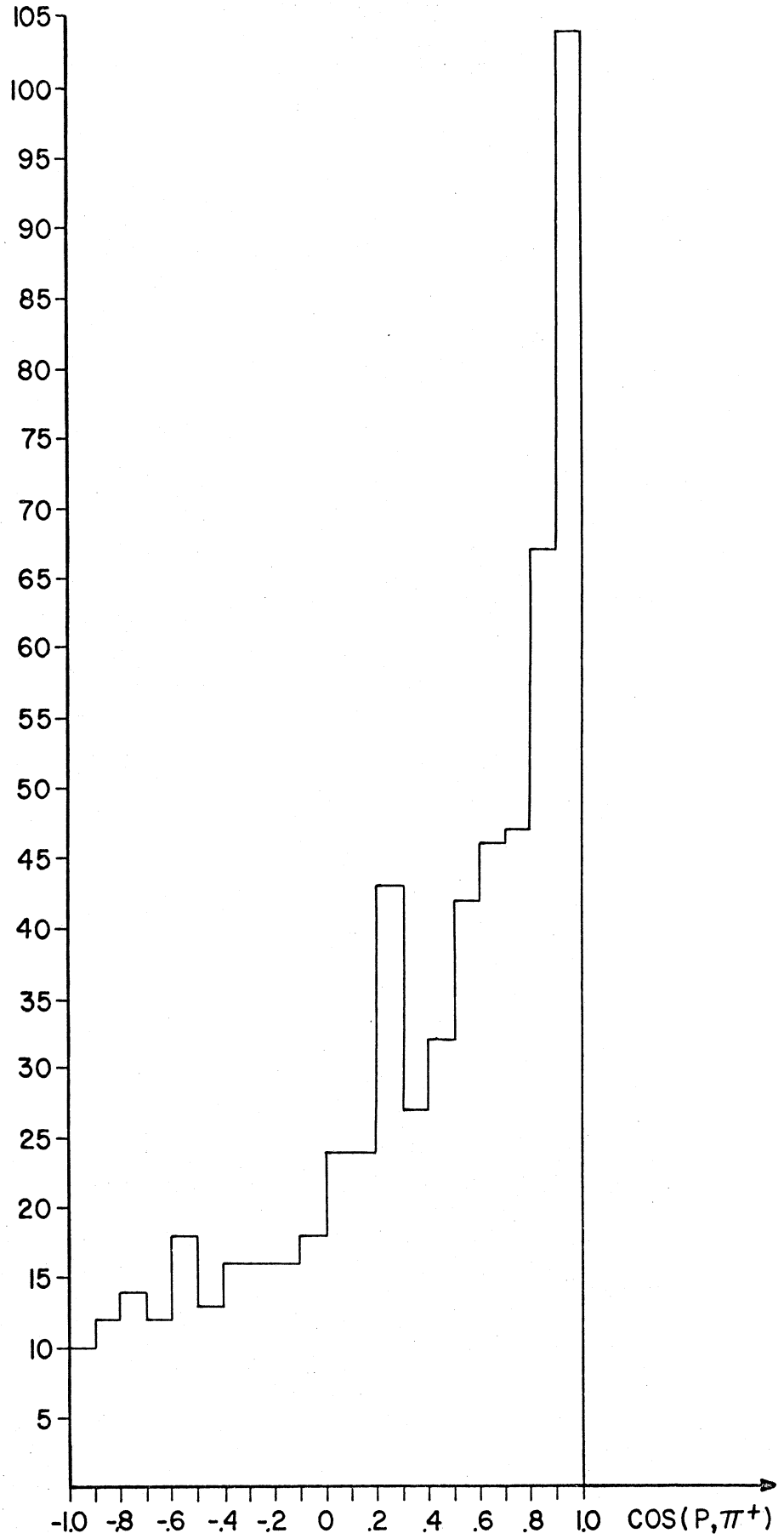

Fig 15. The orientation of the proton with respect to the π^+ beam.

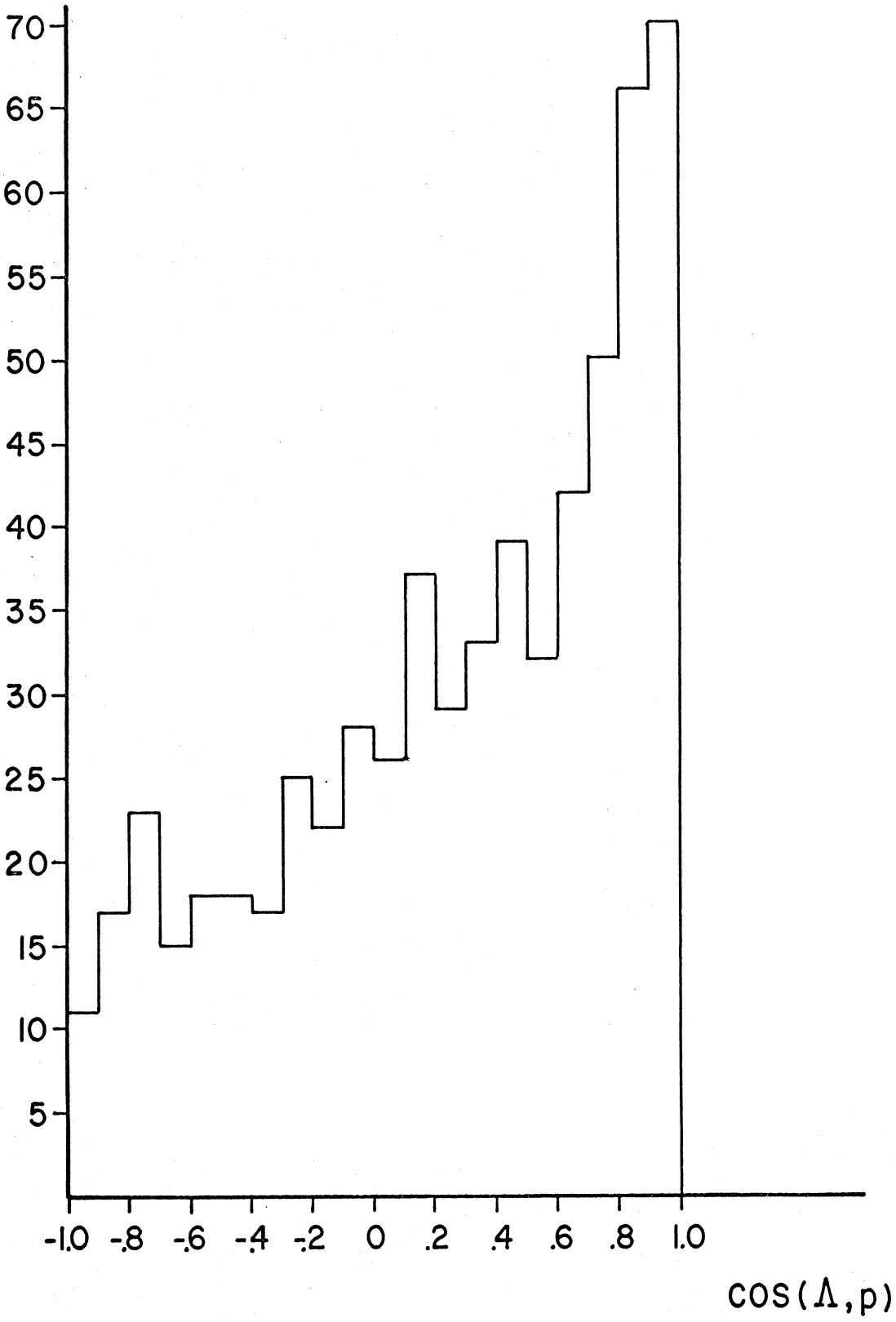

Fig 16. The orientation of the proton with respect to the lambda.

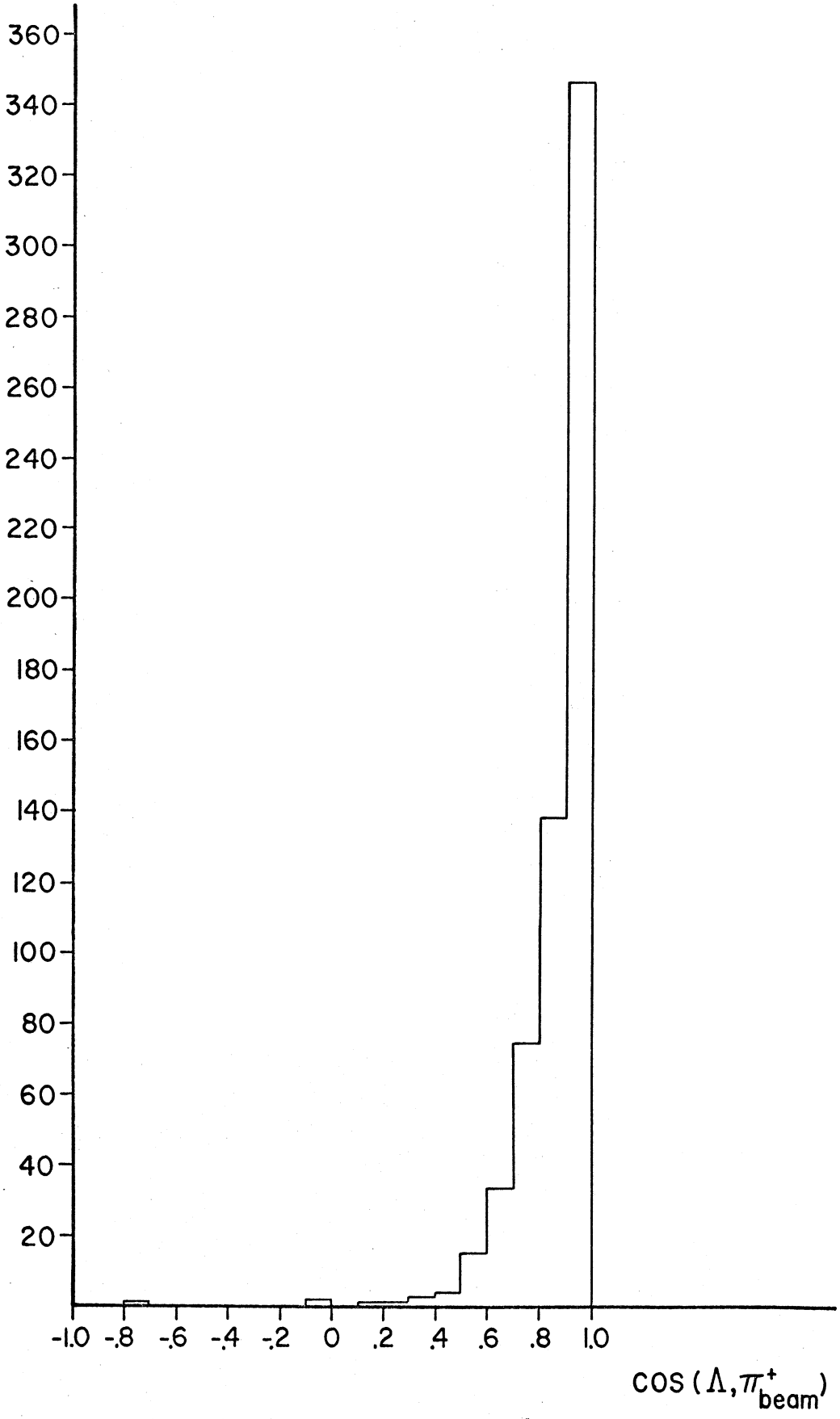

Fig 17. The orientation of the lambda with repect to the beam.

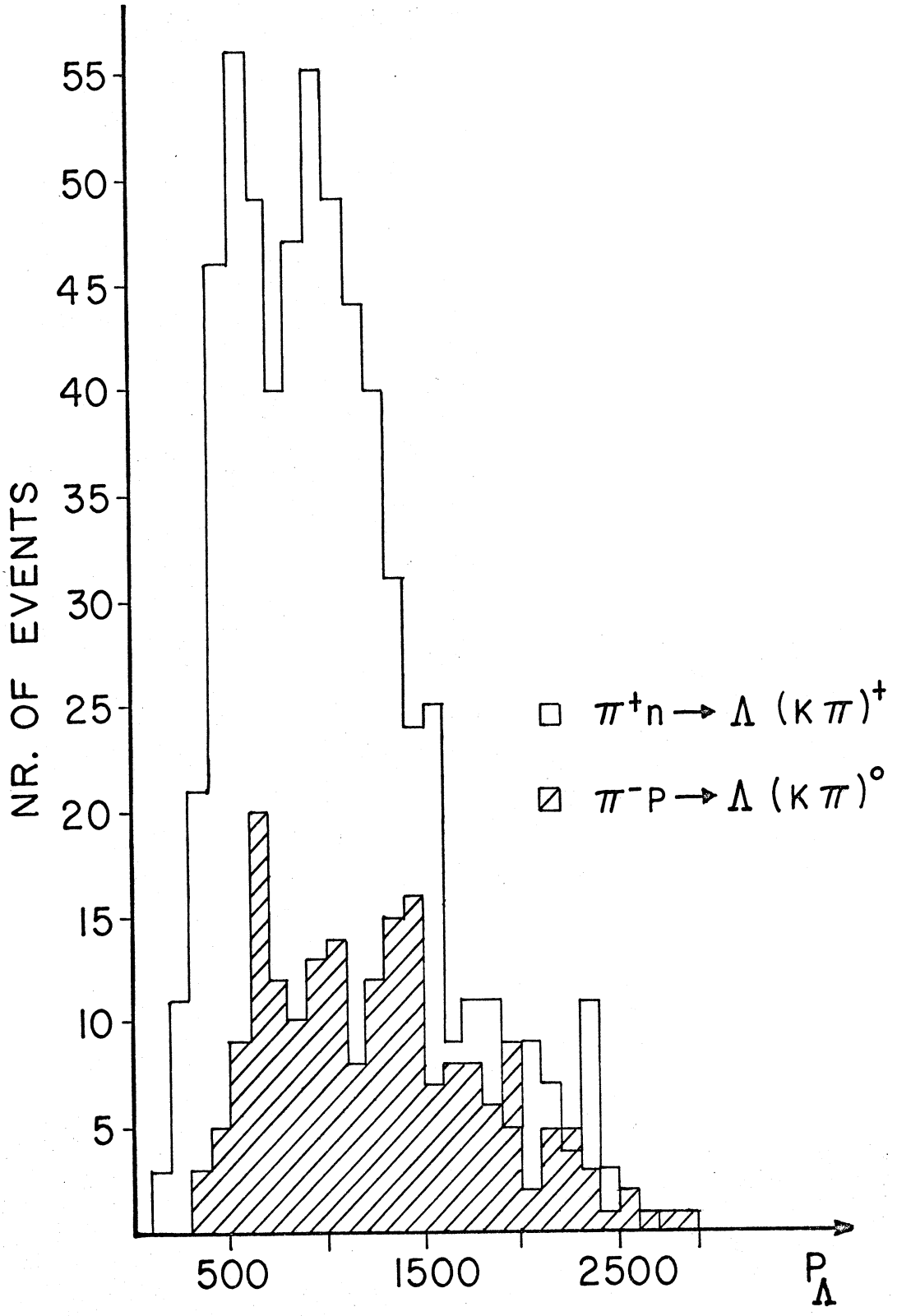

Fig 18. A comparison of the laboratory momentum spectra from the reactions

$$\pi^+ D \rightarrow P\ \Lambda\ K\ (n\pi)$$

and

$$\pi^- P \rightarrow \Lambda\ K\ (n\pi)$$

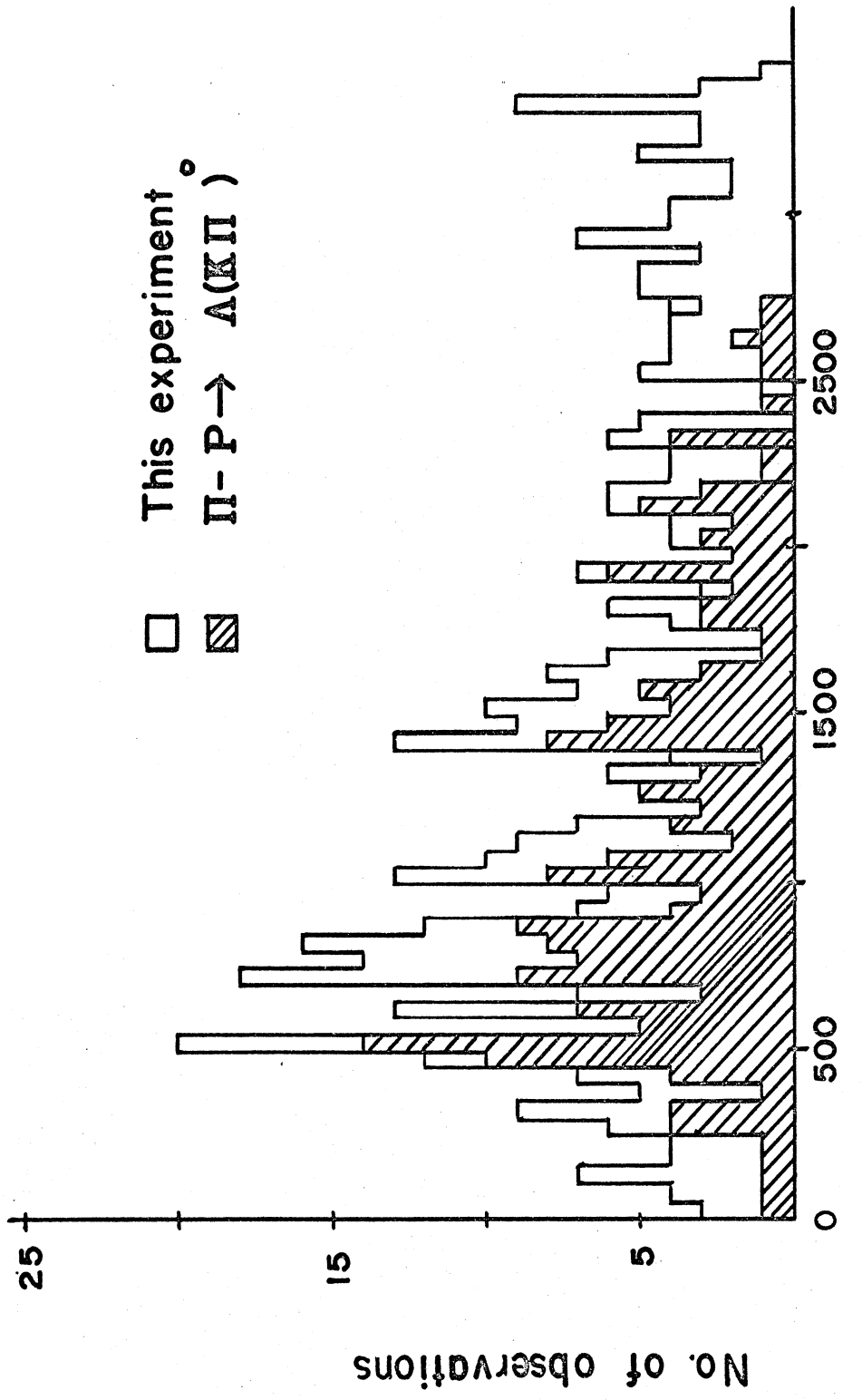

Fig 19. A comparison of the K meson momentum spectra from the reactions π^+ D → P Λ K ($n\pi$) and π^- P → Λ K ($n\pi$)

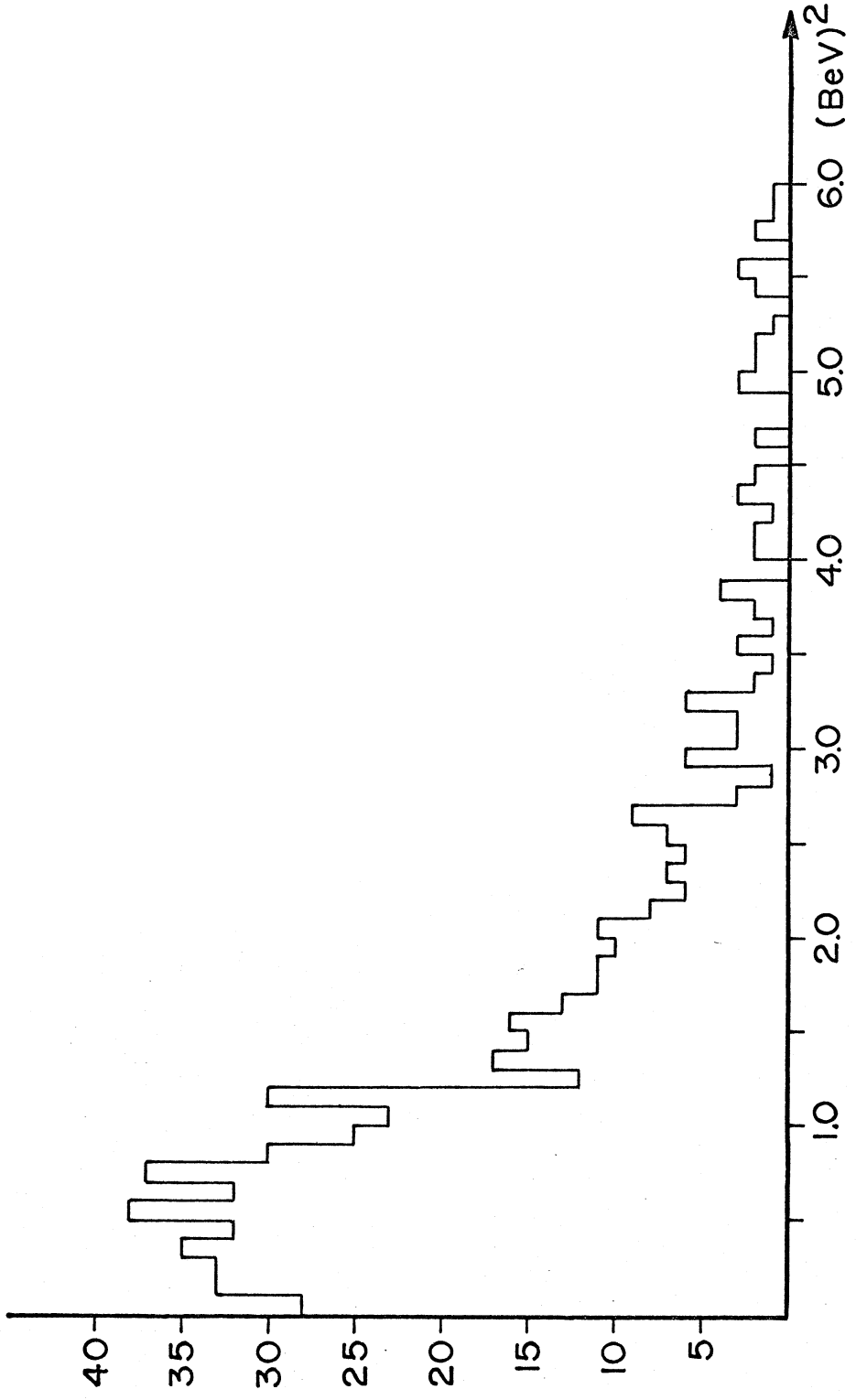

Fig 20. The four momentum transfer Δ^2 from the deuteron to the Λ-P system.

CHAPTER 3

MESON FINAL-STATE INTERACTIONS

3-1. Reduction of Fitted Data

The events were kinematically analyzed by the program GRIND. This program takes the momentum assignments and momentum error assignments of TRED, and, after assigning mass hypotheses to the tracks, applies the laws of conservation of momentum and energy. The method GRIND uses is briefly as follows: The computed momenta must satisfy not only conservation of energy and momenta, but also the condition that χ^2 for the events is a minimum, χ^2 being defined as the weighted mean square deviation of the computed quantities from the measured ones. That is

$$\chi^2 = \sum_{i,j=1}^{n} (P_i - P_i^m)\, G_{ij}^{-1}\, (P_j - P_j^m)$$

where the weighting matrix G_{ij}^{-1} is the inverse of the error matrix

$$G_{ij} = \delta P_i^m \, \delta P_j^m$$

i.e., the product of the measured errors, and

P_i - the fitted values of the momentum
P_i^m - the measured values of the momentum
n - the number of measured variables

Both the requirements of conservation of energy and momentum, and a minimal χ^2 are satisfied simultaneously when one minimizes the expression

$$\chi^2 (P,\alpha) = \chi^2 + \sum_{k=1}^{n'} \alpha_k f_k (P)$$

where the $f_k (P) = 0$ are the n' constraint equations. If the constraint equations were linear in the P_i, the "best fit" momenta would be easily obtained by solving the set of linear equations

$$\partial \chi^2 (P,\alpha) / \partial P_i = 0$$

However, the conservation of energy equation is not linear in the momenta, so that neither is the above set of equations. Hence, since no general way is known to solve non-linear equations, they are first linearized by writing $P_i = P_i^m + \Delta P_i$. and expanding the constraint equations in a Taylor series. Thus, the equations

$$\frac{\partial \chi^2 (P,\alpha)}{\partial \Delta P_i} \doteq 0$$

are soluble and the process may be iterated to obtain a set of momenta which converges to a set satisfying conservation of energy and momentum. The process terminates after 9 steps, or if the process is found to diverge.

In general, there are 4 constraint equations, one for each of the three momentum components and one for the energy. If, however, there is a missing neutral particle, such as a π° , its momentum may be inferred from the conservation of momentum equations and its energy from the relation $E^2 = P^2 + M^2$. Hence, in the case of a missing neutral, energy conservation is the only constraint. A fit of this

kind is called a one constraint, or 1c fit, whereas if there are no missing particles, it is called a 4c fit. There are additional constraints, moreover, which may be applied to V events. Since the direction of the line joining the vertex and the tip of the V must be the same as the direction of the sum of the momenta of the two prongs of the V, there are two additional constraint equations for each V particle. In addition, the momenta of the tracks of the V must satisfy the relation

$$(E_1 + E_2)^2 - (P_1 + P_2)^2 = M_V^2$$

where M_V is the mass of the V. When these three additional constraints are applied, the fit is called an Nopt 2 fit, or in the case of two V's, and hence 6 constraints, Nopt 3. Thus it is possible to have 1c, 4c, 7c, and 10c fits.

In fitting an event, GRIND performs the following sequence of calculations. First, the effective mass of the V is computed along with a χ^2 probability of being a K° or a Λ. Next, a coplanarity test is made on the V to determine if the V particle is associated with the vertex of the event. If so, the event is fitted by adding the prongs of the V to the vertex using the ordinary fitting procedure, thus giving an Nopt 1 fit. Next, the additional constraints are employed, yielding Nopt 2, or Nopt 3 fits.

GRIND tried 55 possible strange particle hypotheses, 22 of which were hypotheses containing a Λ and a proton.

A successful GRIND fit for a given hypothesis includes as output the fitted momenta, errors in momenta and predicted bubble density for the tracks, as well as the χ^2 for the hypothesis. It also includes the number of steps taken to converge and the number of constraints.

Most of the 562 events successfully fitted by GRIND received good fits for several hypotheses. In general, accepting only Nopt 2 or Nopt 3 fits reduced the number of hypotheses, but in order to assign a unique hypothesis, the events were re-examined visually to compare the predicted bubble density with the observed bubble density for all tracks. In this way 235 events receiving Nopt 2 fits were found to have only one GRIND hypothesis which was consistent with the observed bubble density, and 96 remained ambiguous and were separated from the others by the program FILE. The remaining 235 events were run through the program POLISH, whose calculations were the source of the final data.

3-2. Meson-Baryon and Meson-Meson Resonant Reactions.

It is interesting to compare the presence of meson-baryon and meson-meson resonant states in this experiment with resonant states in the π-P data. Wangler (1964), in the reaction

$$\pi^- P \rightarrow \begin{cases} K^\circ \pi^+ \pi^- \Lambda \\ K^+ \pi^\circ \pi^- \Lambda \end{cases}$$

sees a substantial N* (1690) in the Λ-K effective mass spectrum. We have plotted our Λ-K effective mass spectrum from the reaction

$$\pi+ \; D \rightarrow \begin{cases} P \; K^{\circ} \; \pi+ \; \pi- \; \Lambda \\ P \; K+ \; \pi^{\circ} \; \pi- \; \Lambda \end{cases}$$

along with his results in Figure 21. These two reactions are charge symmetric according to the spectator hypothesis. Although the statistics are meager, we see no evidence of the N* (1690). Figure 22 compares the Λ-π effective mass spectra from the same two reactions.

The π-P data shows clearly a Y* (1385) whereas our data does not, although again, statistics are meager. The K-π effective mass spectra from the above reactions, however, shows a clear K* (891) in both the π-P and π+D events. This is shown in Figure 23. Figures 24 and 25 contrast effective mass spectra from the reactions

$$\pi- \; P \rightarrow \begin{cases} K+ \; \pi- \; \Lambda \\ K^{\circ} \; \pi^{\circ} \; \Lambda \end{cases}$$

and

$$\pi+ \; D \rightarrow \begin{cases} P \; K+ \; \pi^{\circ} \; \Lambda \\ P \; K^{\circ} \; \pi+ \; \Lambda \end{cases}$$

which, according to the spectator model, are charge symmetric. Figure 24 shows the K-π effective mass spectra. Both reactions exhibit a strong K* (891). Finally, Figure 25 shows the Λ-π effective mass spectra. Both experiments show a Y* (1385), although it is possible that in our experiment the excess of events above background in the

Y* (1385) region is a reflection of the K* (891). We have shaded events which satisfy

$$1300 \leq M_{\Lambda\pi} \leq 1450$$
$$850 \leq M_{K\pi} \leq 950$$

As shows in Figure 25, the number of such events is roughly equal to the number of events above background.

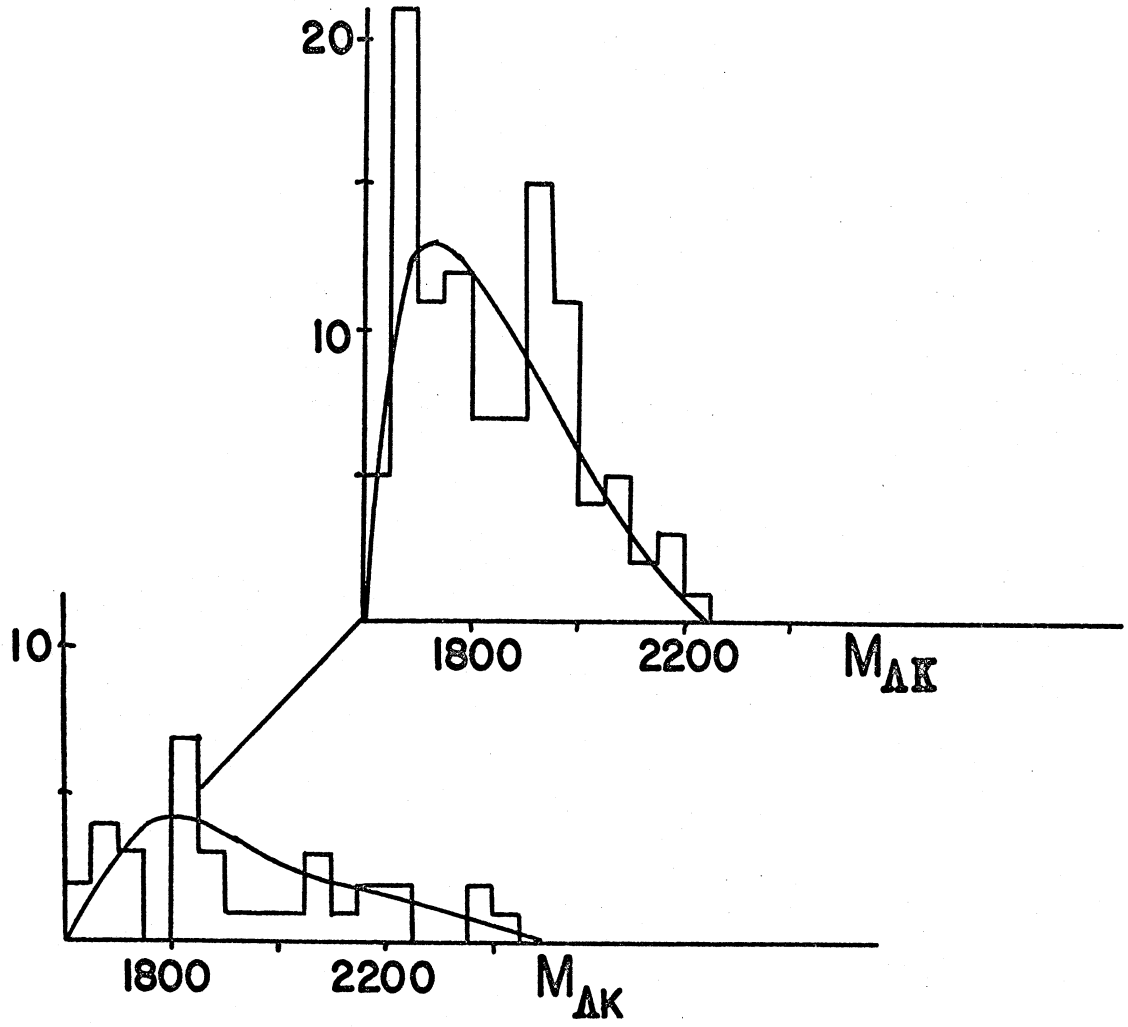

Fig 21. A comparison of the Λ K effective mass spectra from the reactions $\pi^+ D \rightarrow \{^{P\ K^o\ \pi^+\ \pi^-\ \Lambda}_{P\ K^+\ \pi^+\ \pi^-\ \Lambda}$ (lower Fig.)

and the reactions $\pi^- P \rightarrow \{^{K^o\ \pi^+\ \pi^-\ \Lambda}_{K^+\ \pi^o\ \pi^-\ \Lambda}$ (upper Fig.)

The peak in the upper figure is the N* (1690).

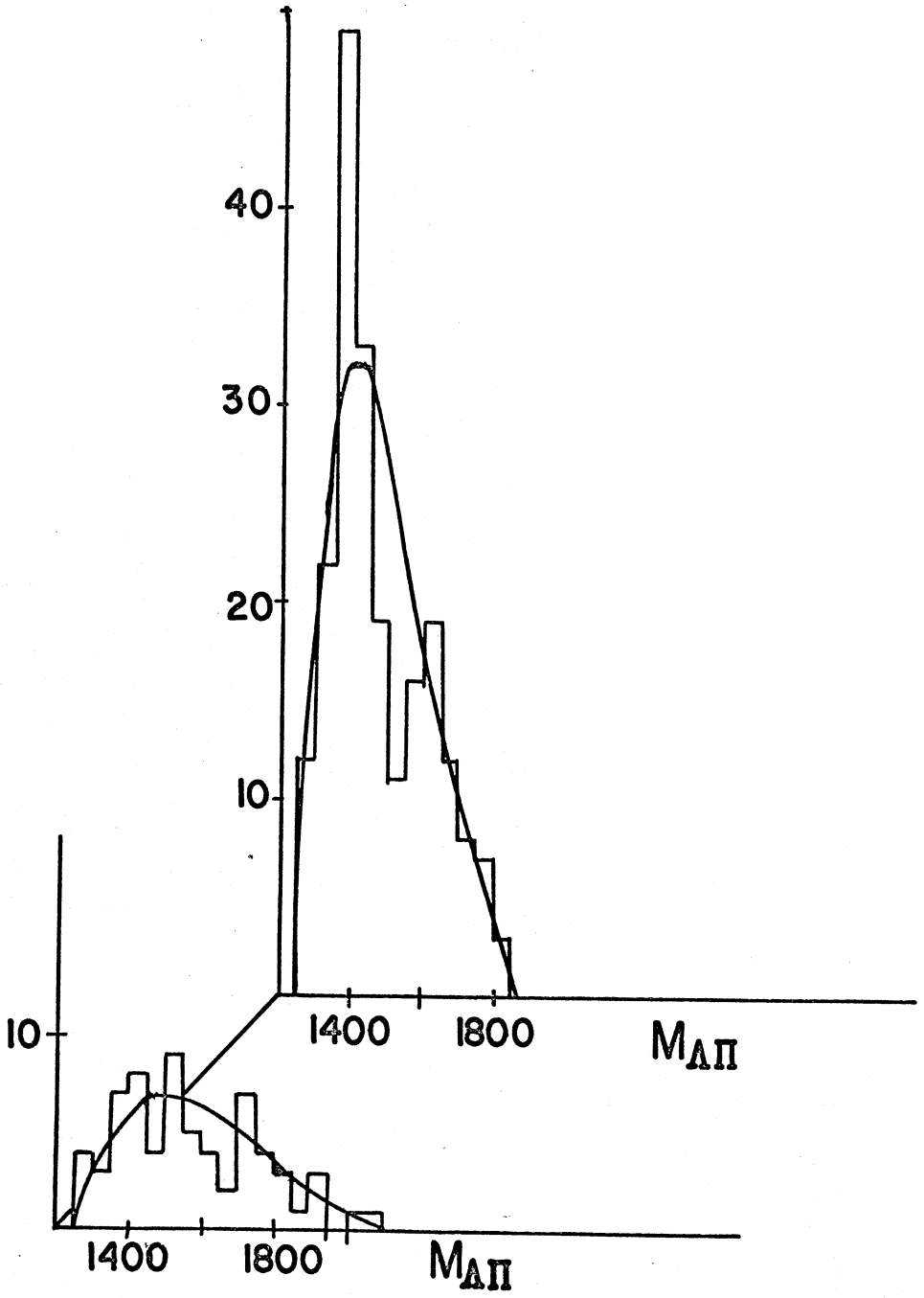

Fig 22. A comparison of the Λ-π effective mass spectra from the reactions

$$\pi^+ D \rightarrow \begin{cases} P\ K^o\ \pi^+\ \pi^o\ \Lambda \\ P\ K^+\ \pi^+\ \pi^-\ \Lambda \end{cases} \quad \text{(lower fig.)}$$

and the reactions

$$\pi^- P \rightarrow \begin{cases} K^o\ \pi^+\ \pi^-\ \Lambda \\ K^+\ \pi^o\ \pi^-\ \Lambda \end{cases} \quad \text{(upper fig.)}$$

The peak in the upper figure is Y*(1385).

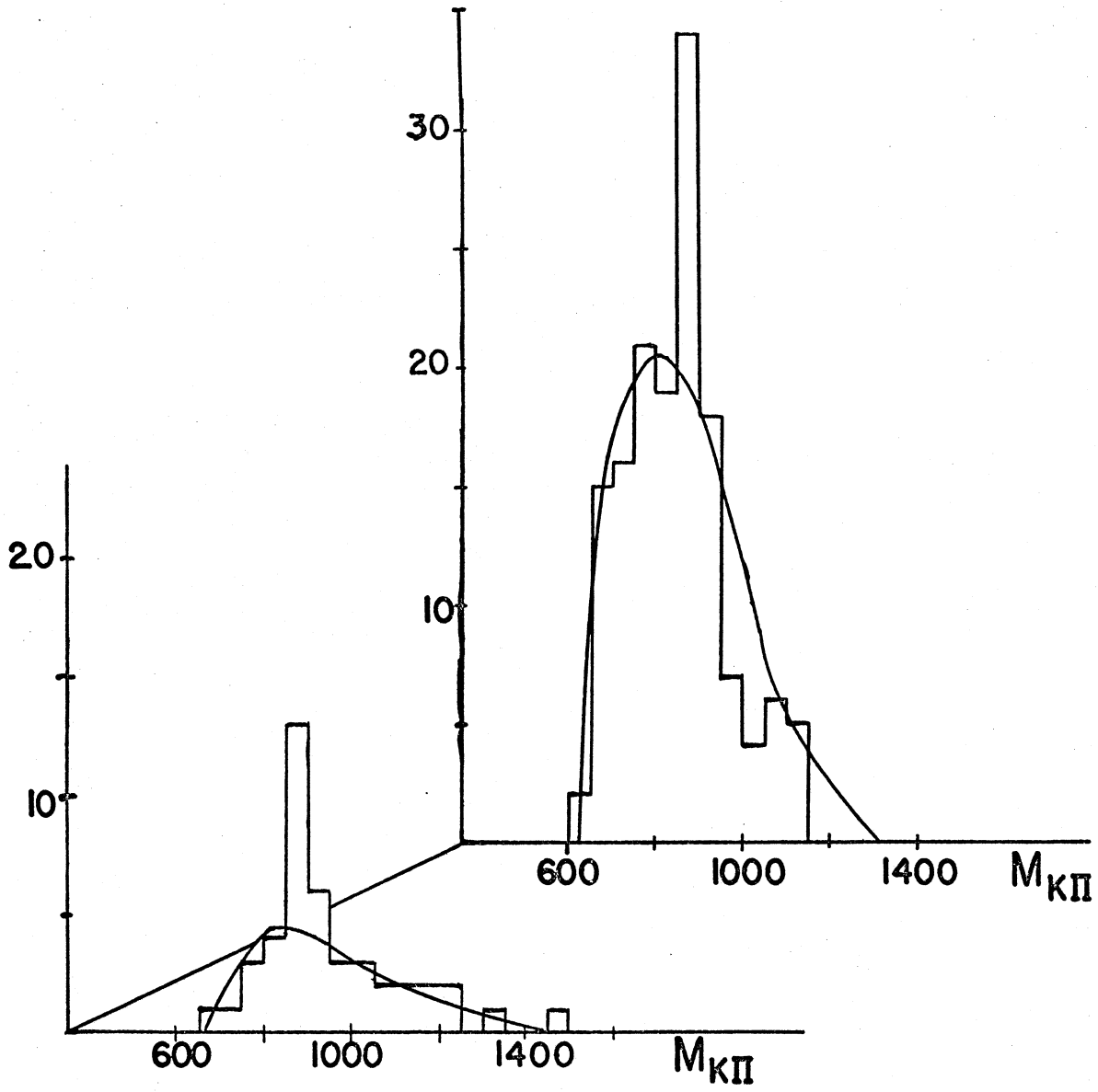

Fig 23. A comparison of the Kπ effective mass spectra in the reactions

$$\pi^+ D \rightarrow \{ {}^{P\ K^o\ \pi^+\pi^o\ \Lambda}_{P\ K^+\ \pi^+\pi^-\ \Lambda} \qquad \text{(lower fig.)}$$

and

$$\pi^- P \rightarrow \{ {}^{K^+\ \pi^-\pi^o\ \Lambda}_{K^o\ \pi^-\pi^+\ \Lambda} \qquad \text{(upper fig.)}$$

The peak in both figures is the k* (891)

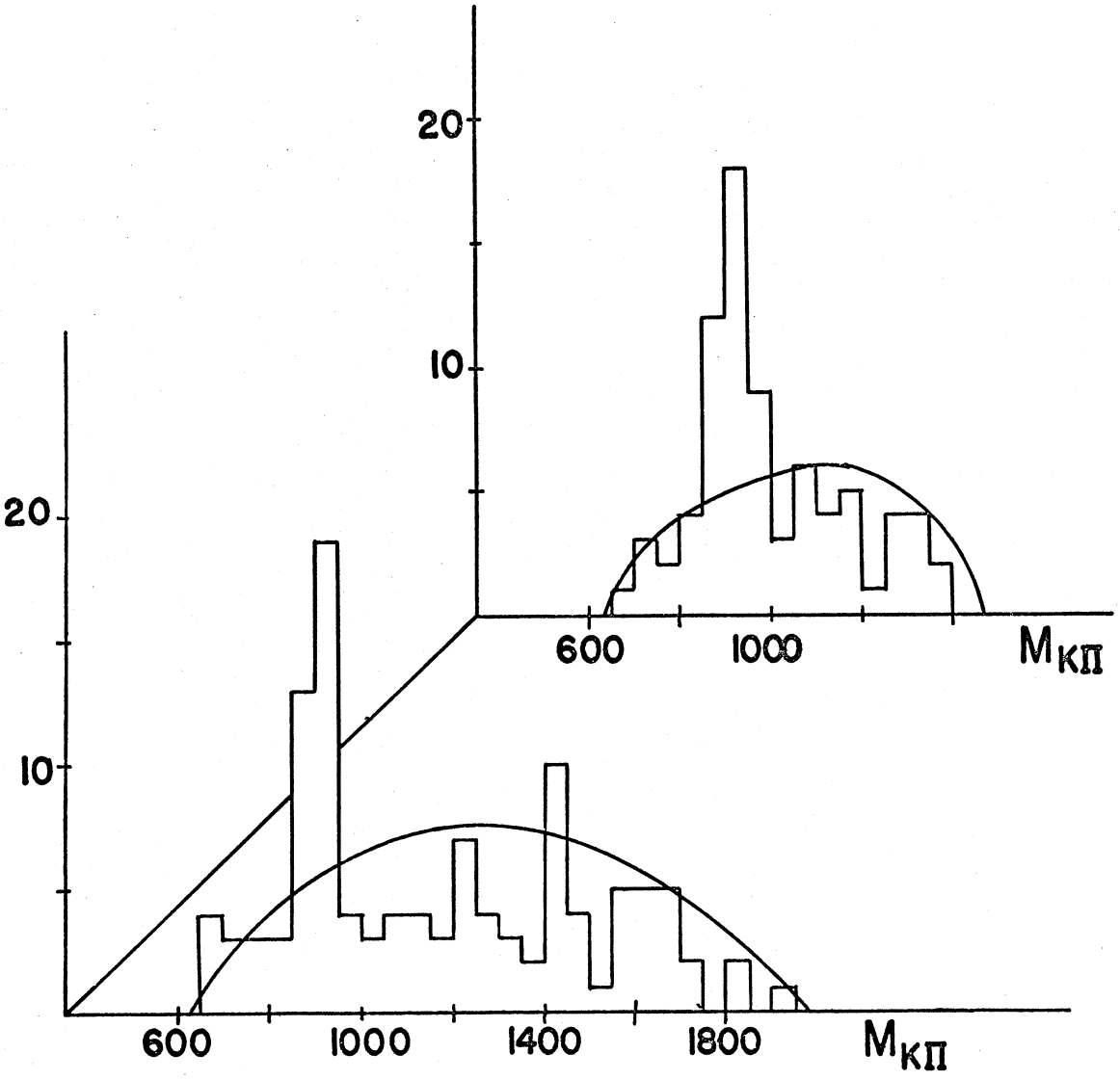

Fig 24. A comparison of the K π effective mass spectra in the reactions

$$\pi^+ D \rightarrow \{ {}^{P\ K^+\ \pi^0\ \Lambda}_{P\ K^0\ \pi^+\ \Lambda} \qquad \text{(lower Fig.)}$$

and $$\pi^- P \rightarrow \{ {}^{K^+\ \pi^-\ \Lambda}_{K^0\ \pi^0\ \Lambda} \qquad \text{(upper figure)}$$

The peak in both figures is the K* (891)

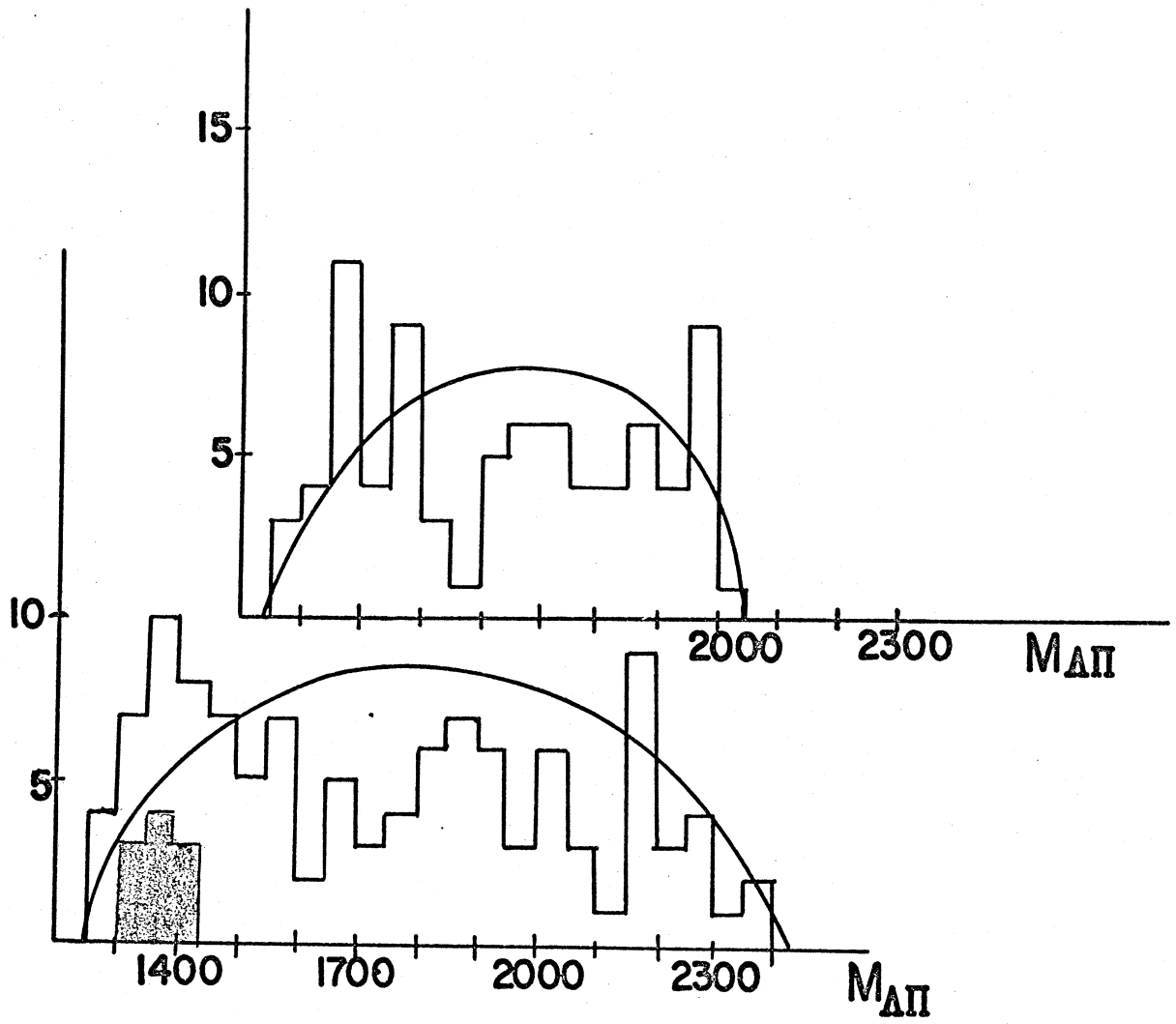

Fig 25. A comparison of the Λ-π effective mass spectra from the reactions

$$\pi^+ D \rightarrow \begin{cases} P\ K^+\ \pi^o\ \Lambda \\ P\ K^o\ \pi^+\ \Lambda \end{cases} \qquad \text{(lower figure)}$$

and

$$\pi^- P \rightarrow \begin{cases} K^+\ \pi^-\ \Lambda \\ K^o\ \pi^o\ \Lambda \end{cases} \qquad \text{(upper fig.)}$$

The shaded events are those for which $850 < M_{K\pi} < 950$ Mev, and $1300 < M_{\Lambda\pi} < 1450$.

CHAPTER 4

RESULTS AND CONCLUSIONS

4-1. The Inadequacy of the Spectator Model.

The spectator model asserts that the nucleon which is not struck by the incident meson does not participate in the interaction. This assertion implies a number of consequences which are inconsistent with experimental results.

First, the proton momentum distribution should be the same after the collision as before. That is, its momentum distribution should simply be proportional to $|\psi(P)|^2 P^2$ where ψ is the wave function of the deuteron in the momentum representation. It was seen in Chapter 2 that the proton momentum distribution was ill-described by the Hulthén theory of the deuteron, which predicted far too few protons with a momentum greater than 225 Mev/c (Figure 14).

Secondly, since there is no preferred direction in the lab, the proton's angular distribution should be isotropic with respect to any fixed direction in the lab. This was shown in Chapter 2 not to be the case. Figure 15 shows many more protons going forward with respect to the beam than backward.

When coupled with the requirement of charge symmetry, the spectator model predicts that the Λ-K-π system in the reaction

$$\pi^- P \rightarrow \Lambda (K \pi)^\circ$$

is identical with the collision products in the reaction

$$\pi+ \; n \rightarrow \Lambda \; (K \; \pi)^{+}$$

for comparable π-N center of mass energy. Due to the fermi momentum of the nucleons there is no unique π-N center of mass energy, but rather it is spread out from 2.6 to 3.1 Bev [Benson (1966)]. However, if we assume a weak dependence of the cross section variation on the center of mass energy, we would expect that the laboratory momentum spectra of the collision products $\Lambda + (K \; \pi)^{\circ}$ in general, and the Λ laboratory momentum spectrum, in particular, to be comparable to those observed in $\Lambda \; (K \; \pi)^{+}$. This is seen not to be the case for the Λ spectrum (Figure 18). The lambdas produced in this experiment are somewhat slower than those produced in the $\pi-$ P experiment of Wangler, even though the average effective beam momentum used in this experiment is slightly higher.

Finally, the two-body effective mass spectra in the $\Lambda \; (K \; \pi)^{\circ}$ system should be the same as those in the $\Lambda \; (K \; \pi)^{+}$ system as regards the production of resonances.

Although the meson-meson resonant states $K^{*} \; (891)^{+}$ and $K^{*} \; (891)^{0}$ proved to be as prominant in $\pi+$ D as in $\pi-$ P, this was not true for the $Y^{*} \; (1385)$. Moreover, no $N^{*} \; (1690)$ was observed in the Λ-K effective mass spectrum. However, the failure to detect strong $N^{*} \; (1690)$ and $Y^{*} \; (1385)$ signals may well be due to meager statistics.

Thus, there is considerable evidence to indicate that the spectator model is not completely valid and that the nucleon that is not struck initially does indeed subsequently participate in the interaction. It is to this question we now turn.

4-2. The Λ-P Interaction.

A number of possible resonances in the Λ-N system have been reported by various researchers. Melissinos et al (1965), after examining the spectrum of K+ mesons in P-P collisions, found the indication of a singularity in the Λ-P S matrix near the Λ-P threshold. The energy above threshold of the singularity was given as

$$Q = +4 \ {}^{+10}_{-5} \text{ Mev}$$

A resonance with half width

$$\Gamma / _2 \cong 15 \ {}^{+10}_{-5} \text{ Mev}$$

is one interpretation of this singularity.

Piroue et al (1964) observed anomalies in the K+ momentum spectrum resulting from the bombardment of a beryllium target by protons. One explanation is a resonance in the Λ-P system at an effective mass of 2360. No attempt was made to assign a width.

Buran et al (1966) observed the Λ-P effective mass spectrum in K- capture on complex nuclei (CF_3 Br).

They report an enhancement at 2220 Mev, the width being estimated at 20 Mev.

By examining the Λ-n effective mass spectrum resulting from K- absorption at rest in helium, Cohn et al (1964) report a resonance at 2098 Mev with a width of 20 Mev.

Figure 26 shows the Λ-P effective mass spectrum for our experiment plotted against a background of non-interacting events which was computed, according to the spectator model, as follows: Proton-neutron pairs were generated with equal and opposite momenta distributed according to a Hulthén probability density. In the rest frame of the neutron, lambdas were created with a momentum distribution given by that in the experiment of Wangler:

$$\pi^- P \rightarrow \Lambda + (K \pi)^\circ$$

A Lorentz transformation was then performed to carry the lambda momentum into the lab and the effective mass of the Λ-P system was computed. A visibility criterion to be described below was applied to the proton, and those events deemed to be visible were histogrammed.

Approximately 15,000 events were thus generated, of which one-third were adjudged visible. The smooth curve drawn through the histogram of visible events is shown in Figure 1.

The visibility criterion is as follows: A particle

of momentum P leaves an ionized track of length R given by a range energy relation

$$R = b\ P^m$$

where in deuterium

$$b = 1036$$
$$m = 3.615$$

The units of b are such that R is in cm when P is in Bev/c. The length projected on the window of the bubble chamber is approximately the length seen by the scanners and depends on the orientation of the particle trajectory with respect to the plane of the window. This is always less than or equal to the length of the track. As shown in the appendix the probability of having a projected length greater than a minimum length R_{min} is

$$Pr = \sqrt{1 - \left(\frac{R_{min}}{R}\right)^2}$$

By multiplying the visibility probability by the Hulthén momentum probability density, a momentum distribution is obtained which predicts the shape of "spectator" proton distribution which will be picked up by the scanners. As discussed in the appendix, we chose the value $R_{min} = .14$ cm since this value yielded a momentum distribution curve which agreed with the spectator proton distribution of an earlier experiment.

For each generated event the above probability was calculated and compared with a random number between 0 and 1.

Those events for which the probability was larger than the random number were deemed visible.

The Λ-P efffective mass curve as seen in Figure 26 reveals none of the above mentioned resonances. However, there is a large accumulation of events above background in the region of 2125 Mev.

As expected, the curve of figure 26 disagrees badly with the data, indicating the failure of the pure spectator model. The disagreement is most pronounced for the low effective mass events, and implies that the low effective mass Λ-P systems interact more readily.

Since the Λ-P elastic scattering cross section decreases as a function of energy, as shown in Figure 1 in Chapter 1, one might suspect that the deviation from the spectator model might be accounted for by the elastic scattering between the lambda and the proton.

The background curve of Figure 26 is not a phase space for the Λ-P system since it is not proportional to the number of events in an effective mass interval which are capable of interacting. Figure 27 shows the Λ-P effective mass of the 10,000 events generated in the same way as those mentioned above, but deemed invisible. According to this curve, there is a large phase space for Λ-P events in the region 2100 - 2200 Mev. Thus, according to this model there is an extreme sensitivity to any interaction in this effective mass region.

In Figure 28 we have calculated percent interaction in this effective mass range. The percent interaction is defined as the percentage of the invisible events which must be added to the visible events to reproduce the experimental data. It is presumed that events in which the Λ interacts with the proton yield a visible proton. The normalization is such that 100% of the events in the mass interval 2050 - 2075 are presumed to interact. The errors are statistical only. One might expect that this curve would be proportional to the total elastic Λ-P cross section if this was solely responsible for the spectator's role in the interaction.

Figure 29 shows the same percent interaction points normalized so that the 2075 point falls on the Λ-P elastic scattering curve of Ali (1967). This curve was calculated to the best fit (according to a least squares criterion) to the low energy Λ-P elastic scattering data. We see from this that, according to this analysis the percent interaction points are, within errors, consistent with Λ-P elastic scattering results, which show a smooth non-resonant variation with energy. Although this procedure does seem to describe events with $M_{\Lambda P} < 2200$, it fails to do so for the higher effective mass events, for which it predicts more events to be visible than are actually observed.

Moreover, such an analysis makes certain predictions

about the proton momentum spectrum as a function of the Λ-P effective mass.

Although the exact Λ-P elastic scattering angular distribution is not known, as discussed in Chapter 1, the experimental data in the region $400 < P < 1500$ Mev/c, ie, with an effective mass satisfying $2085 < M_{\Lambda P} < 2370$ Mev, shows an angular distribution consistent with isotropy.

We have fed in the hypothesis of isotropic scattering in the Λ-P center of mass and calculated the resulting laboratory proton momentum spectrum. Figure 30 shows the experimental momentum spectrum compared with that predicted by assuming no interaction (the spectator model) and the momentum spectrum predicted by S wave (i.e., isotropic) scattering. The spectator curve is normalized at the momentum value 100 Mev/c, whereas the S wave scattering curve is normalized in accordance with Figure 28. That is, 100% of the events in the effective mass interval 2050 - 2075 Mev are presumed to have S wave scattered, 50% in the interval 2075 - 2100 Mev, etc. The results show generally poor agreement above 2100 Mev indicating that this method of analysis is not free from internal inconsistency.

One interesting feature of the data is the large number of events in the 2100 - 2125 Mev range in which the proton momentum lies between 100 and 200 Mev/c.

These events may be due to an interaction characterized by a peripheral angular distribution, or they may be spectator events.

In an attempt to determine what sort of distribution must be assumed to account for these events we have calculated the angular distribution of the events whose effective mass lies between 2100 and 2125 Mev under two separate assumptions: First, we have calculated the cosine of the angle made by the Λ in the Λ-P rest frame with the direction of the β communicating with the laboratory frame. This angle is the scattering angle, i.e., the angle between the initial and final Λ direction in the Λ-P center-of-mass if the proton is initially at rest in the laboratory.

We have generated background events by calculating the cosine of the same angle with visible Hulthén protons replacing the experimental protons. Figure 31 (a) shows the angular distribution with a background curve normalized to 51% of the slow proton events ($P_p < 225$ Mev/c), or, 19 events (see Figure 16). By subtracting 19 background events, we obtain the angular distribution shown in Figure 31 (b).

For comparison, we have superimposed a curve describing n-P elastic scattering at a proton momentum of 575 Mev/c. [This curve was taken from the work of Hess (1955)]. Figure 32 shows the same scattering angle, now smeared in a statistical manner, under the assumption that the proton before

the collision is distributed isotropically in the laboratory with its momentum distributed according to a Hulthén probability density.* Ten initial protons were generated for each final proton, and the cosine of the angle between the initial and final proton was calculated. The result, along with a background curve similar to that shown in Figure 31 (a), but normalized to 190 events, is shown in Figure 32 (a). Figure 32 (b) shows the angular distribution with the 190 background events subtracted. The n-p elastic scattering angular distribution is also shown. It is clear from both Figure 31 (b) and 32 (b) that after a background subtraction is made, the angular distribution is comparable to the n-P distribution in the forward region.

Thus, we conclude that the peak in the Λ-P mass spectrum (Figure 26) at 2100 - 2125 Mev is consistent with being made up of 26% non-interacting Λ-P events and of 74% events in which the Λ elastic scatters off the proton with an angular distribution similar to that shown in Figures 31 (b) and 32 (b).

It is possible that the basic assumption that the Λ momentum spectrum is a slowly varying function of the π-n center of mass energy is not valid. For this reason another

* This distribution is shown in Appendix 1, Figure 36.

background curve, independent of Wangler's data was calculated as follows: Our experimental Λ's from events whose proton momentum lay below 225 Mev were compounded with Hulthén protons. Although some of these Λ's may have interacted, it is believed that any interaction undergone will not alter the Λ momentum spectrum appreciably, since the protons associated with these events are not fast enough to be inconsistent with the spectator model. Figure 33 shows the experimental Λ-P effective mass spectrum along with the curve, so calculated, depicting the non-interaction background in which only events deemed visible by the aforementioned visibility criterion are employed. The curve results from drawing a smooth curve through the histogram of of approximately 6,000 events, and normalizing so that the area enclosed equals the experimentally observed number of events. Any inconsistency of the curve and the data must then be reflected in a departure of the observed proton spectra from the Hulthén prediction for $P_p < 225$ Mev/c. That this is indeed so for the $M_p = 2100 - 2125$ region can be seen In Figure 30. The enhancement at 2125 Mev is dramatically in evidence among the slower proton events. This is not inconsistent with the findings of Cohn et al, whose nucleons were slow enough to be consistent with a spectator model. The lower effective mass value (2198 Mev) observed might be due to the upper kinematic limit of 2100 Mev in their experiment.

In Figure 34 we show the Λ-P effective mass spectrum for the events whose proton momentum is in the interval $100 < P_p < 225$ Mev/c. This figure shows the enhancement centered at 2125 Mev to have a width at half-maximum of 40 Mev. Since this enhancement occurs so close to the Σ-N threshold at 2130 Mev, it is possible that the excess events are the result of the interaction of the Σ-N system with the Λ-P system. This possibility is explored in Appendix II where cusp phenomena and Σ-Λ conversions are discussed.

4-3. Summing Up

In conclusion, a number of observations can be made. First, the spectator model is not completely valid for Λ-P events. Secondly, there seems to be a vigorous interaction between the lambda and proton in the effective mass region of 2100 - 2150 Mev. Moreover, this interaction is not accounted for by a monotonic decrease in the elastic scattering cross section as a function of energy. Since this interaction is most readily apparent among the slower proton events ($P_p < 225$ Mev), it is not pure S wave in nature (Figure 30), but must contain a forward peak in the center-of-mass angular distribution (Figures 31 and 32).

The enhancement whose center is at 2125 Mev and whose width at half maximum is 40 Mev is possibly related to the presence of the Σ-N threshold at 2130 Mev. The detailed investigation of this enhancement will probably have to

await the accumulation of large statistics in the scattering of lambdas near 600 Mev/c off free protons.

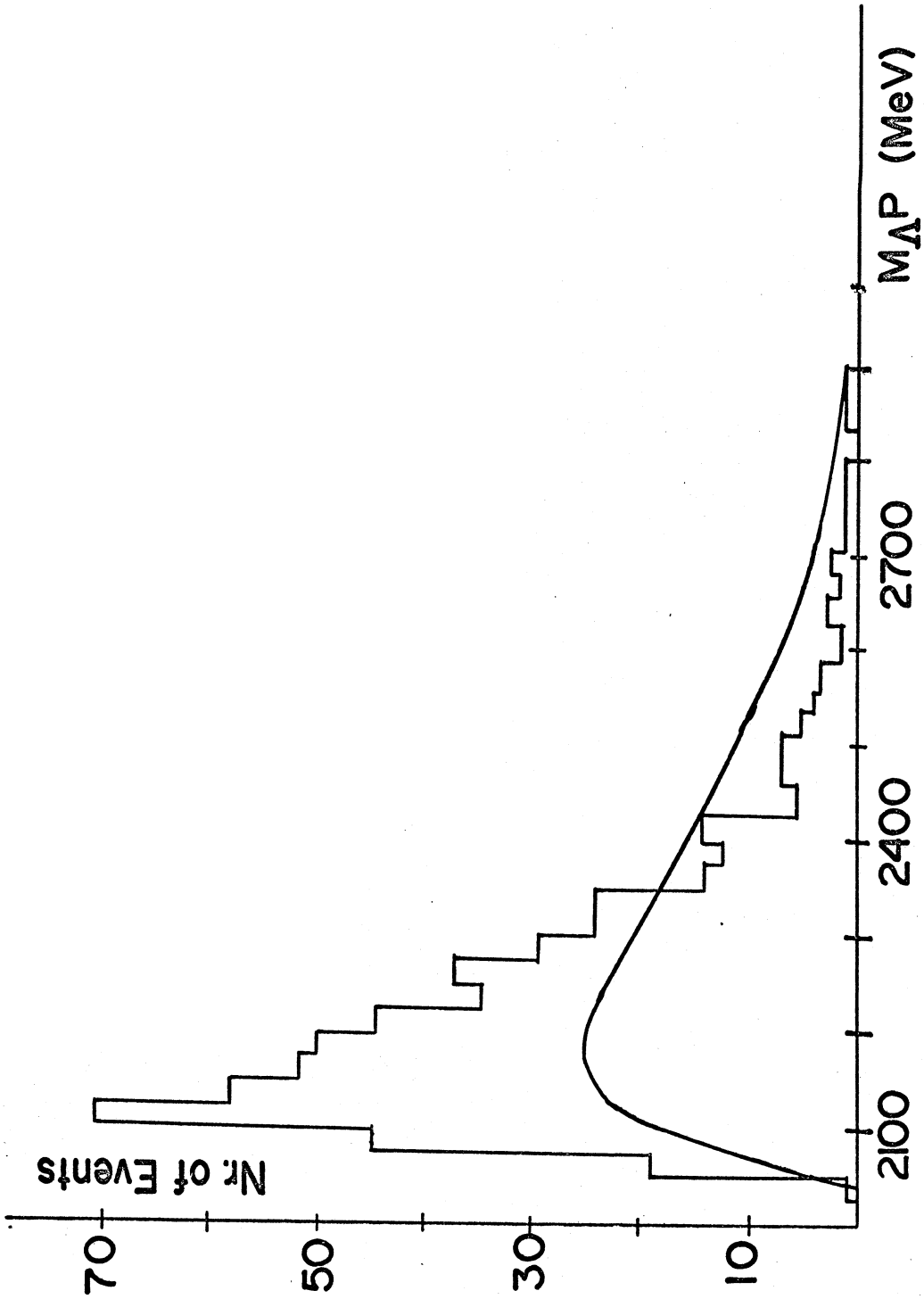

Fig 26. The Λ-P effective mass spectrum. The background curve, a prediction of the spectator model, is described in the Text.

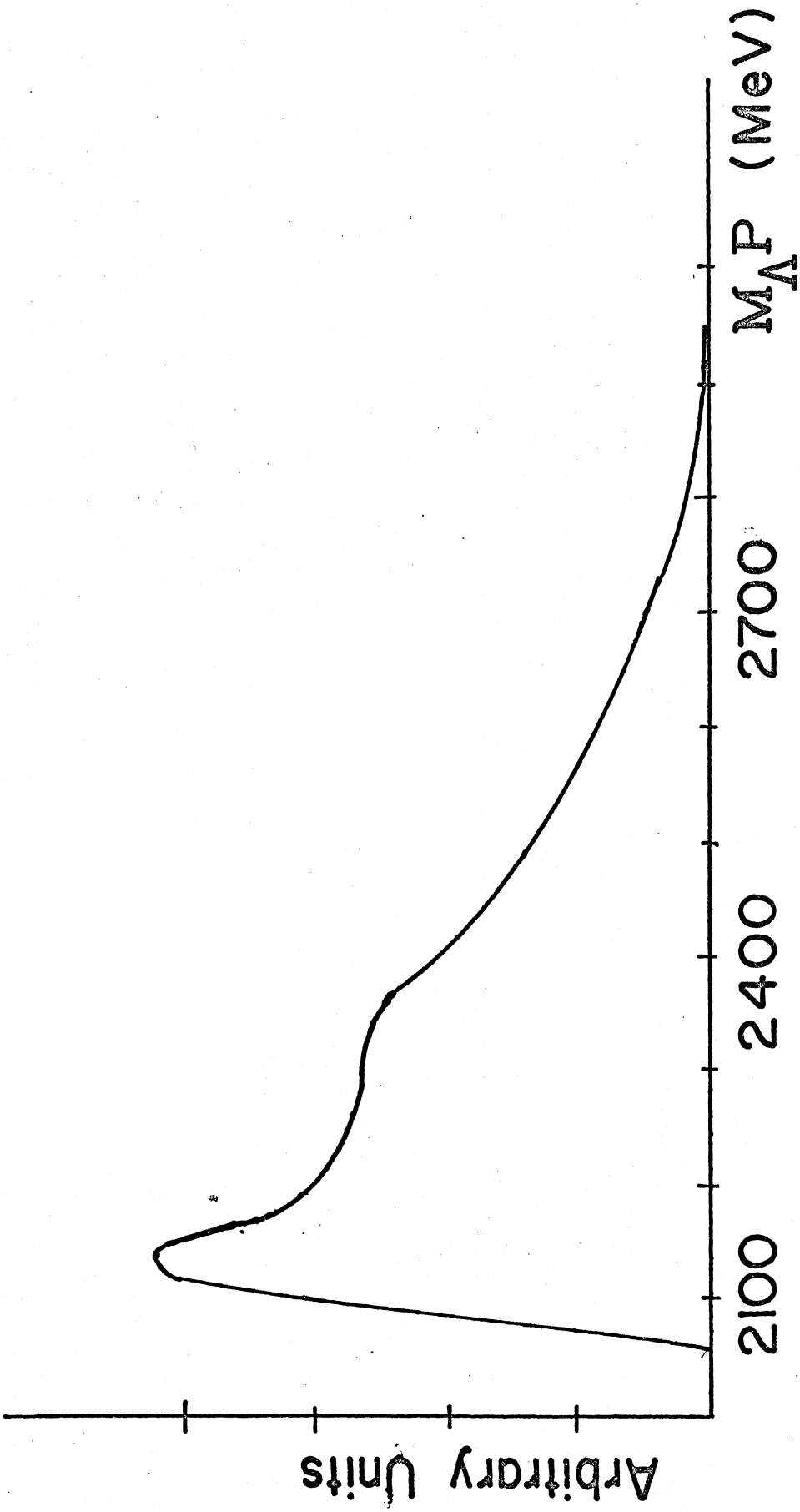

Fig 27. The invisible events. This curve, described in the Text, is proportional to the number of events in which the proton is not observable.

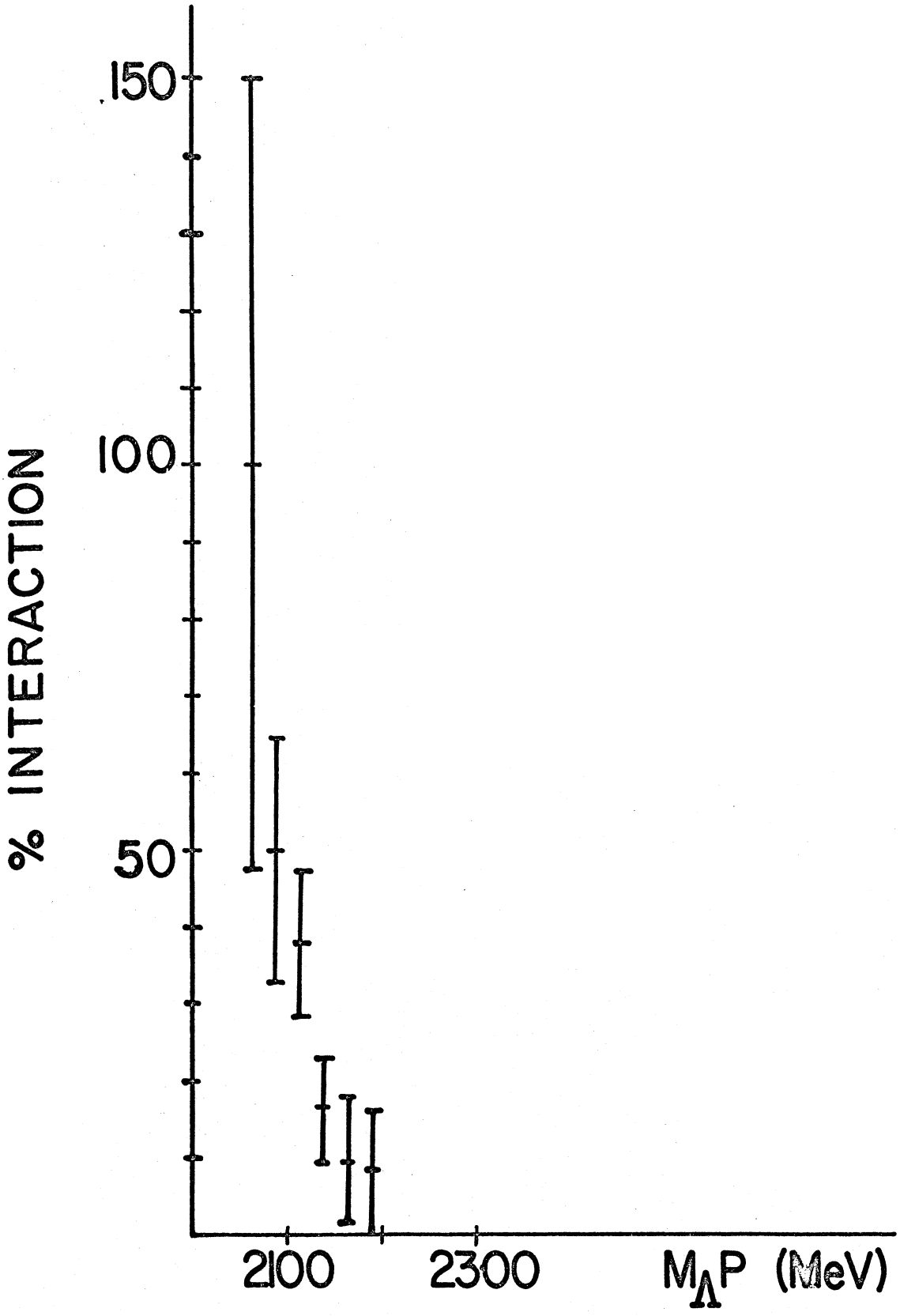

Fig 28. The percent interaction as a function of $M_{\Lambda P}$. This figure is described in the Text.

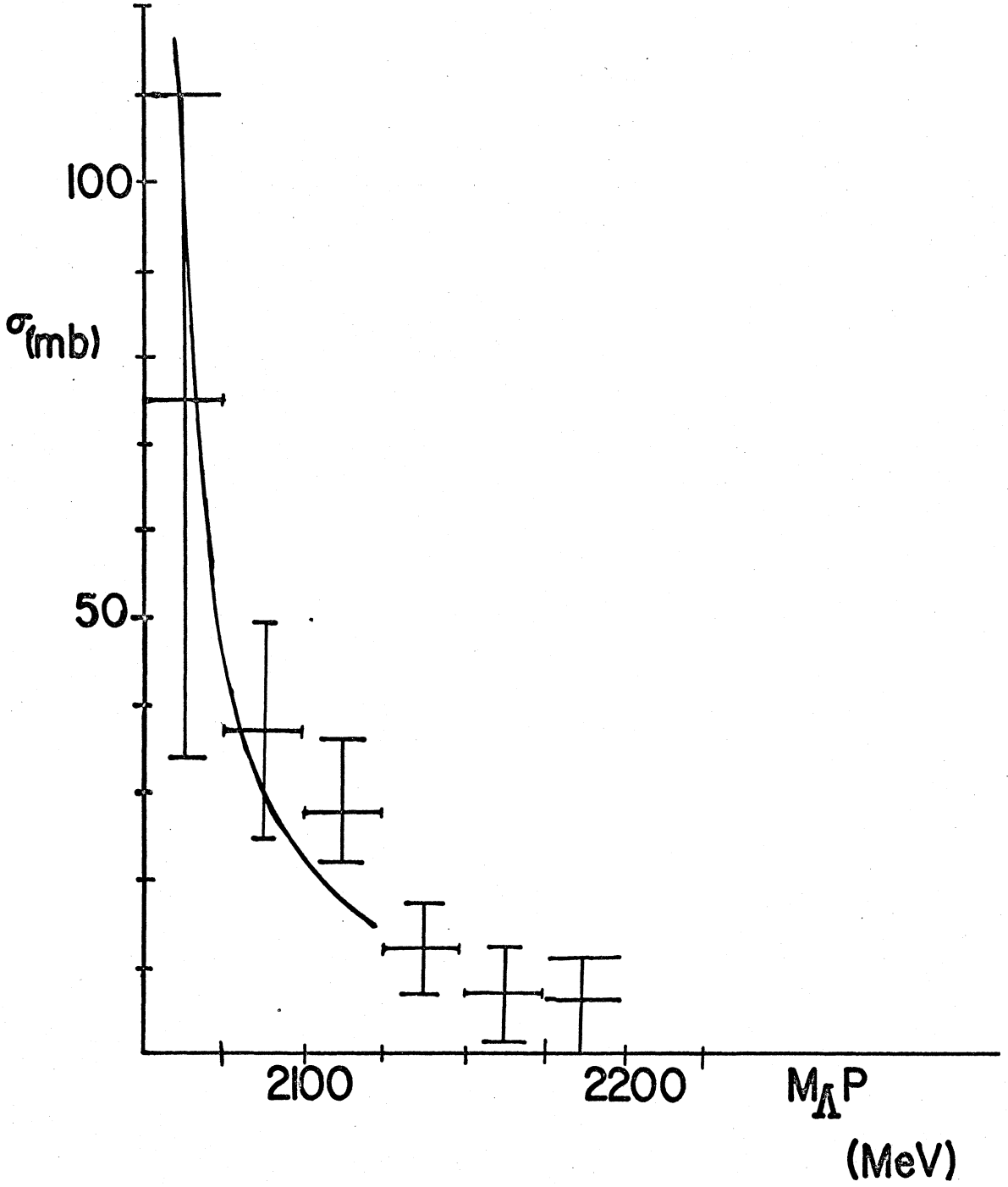

Fig 29. The percent interaction is compared with Λ-P elastic scattering behavior.

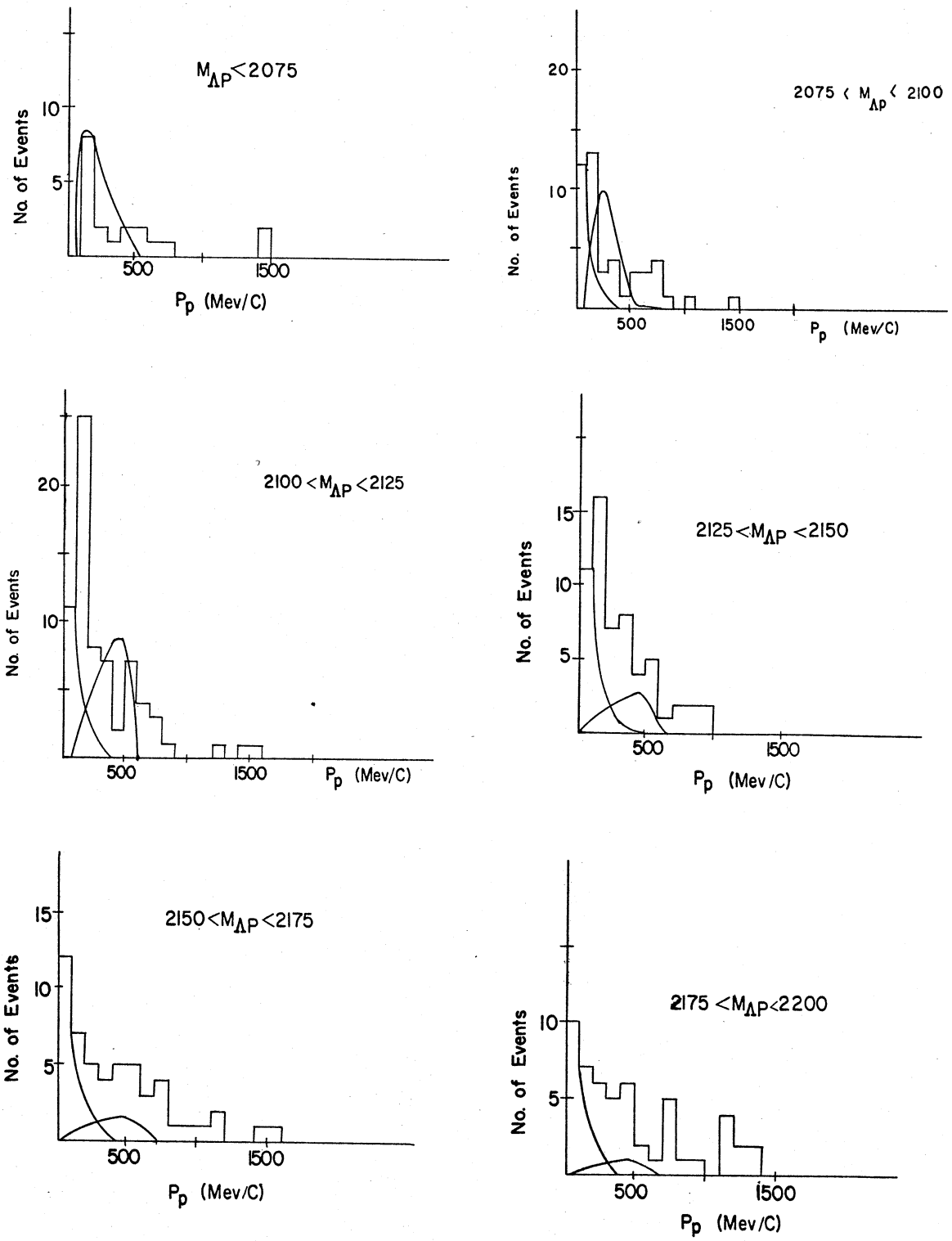

Fig 30. The proton momentum spectra as a function of $M_{\Lambda P}$. The curves represent the predictions of the spectator model and a model of isotropic ΛP scattering in the center of mass.

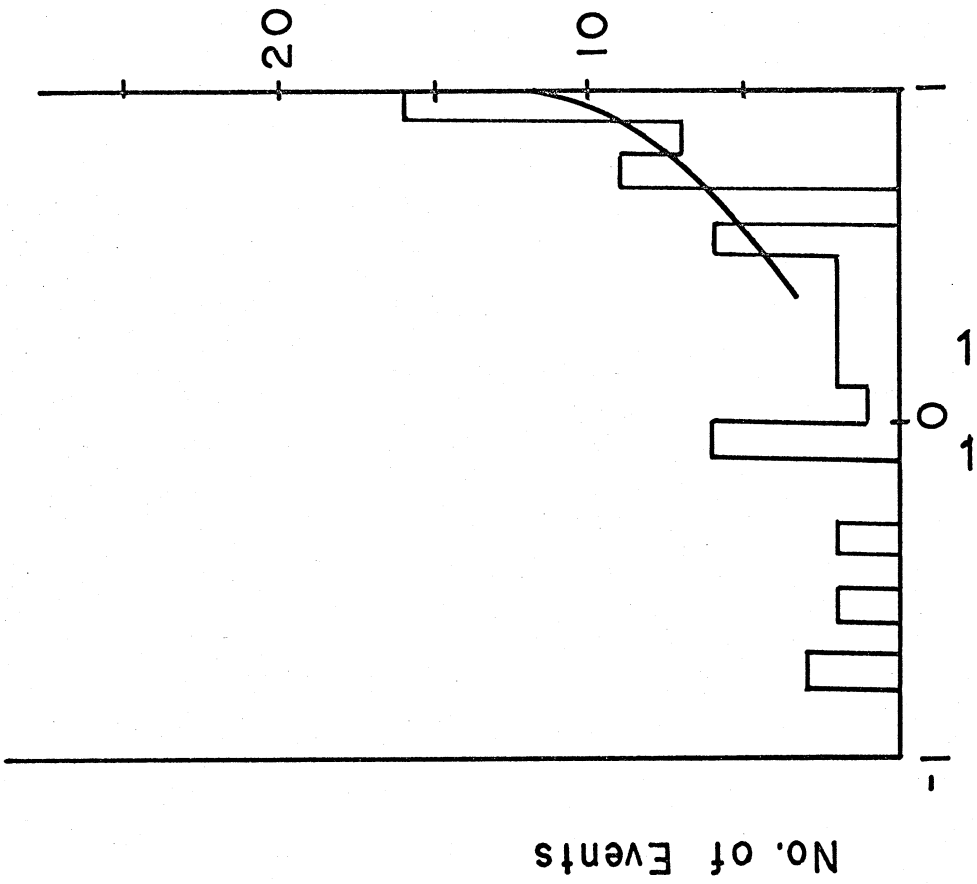

Fig 31.a The scattering angle in the in the center of mass assuming the proton is initially at rest.

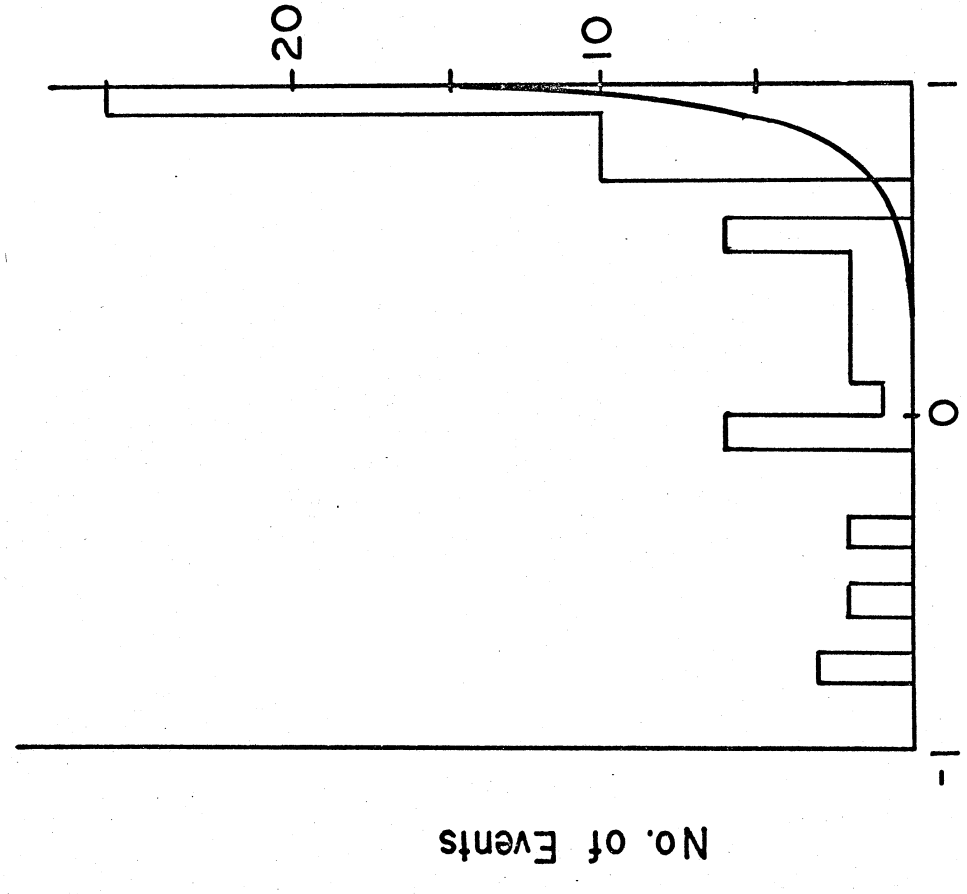

Fig 31.b The angular distribution of fig 31.a after a background sutraction. The results are compared with n-p elastic scattering.

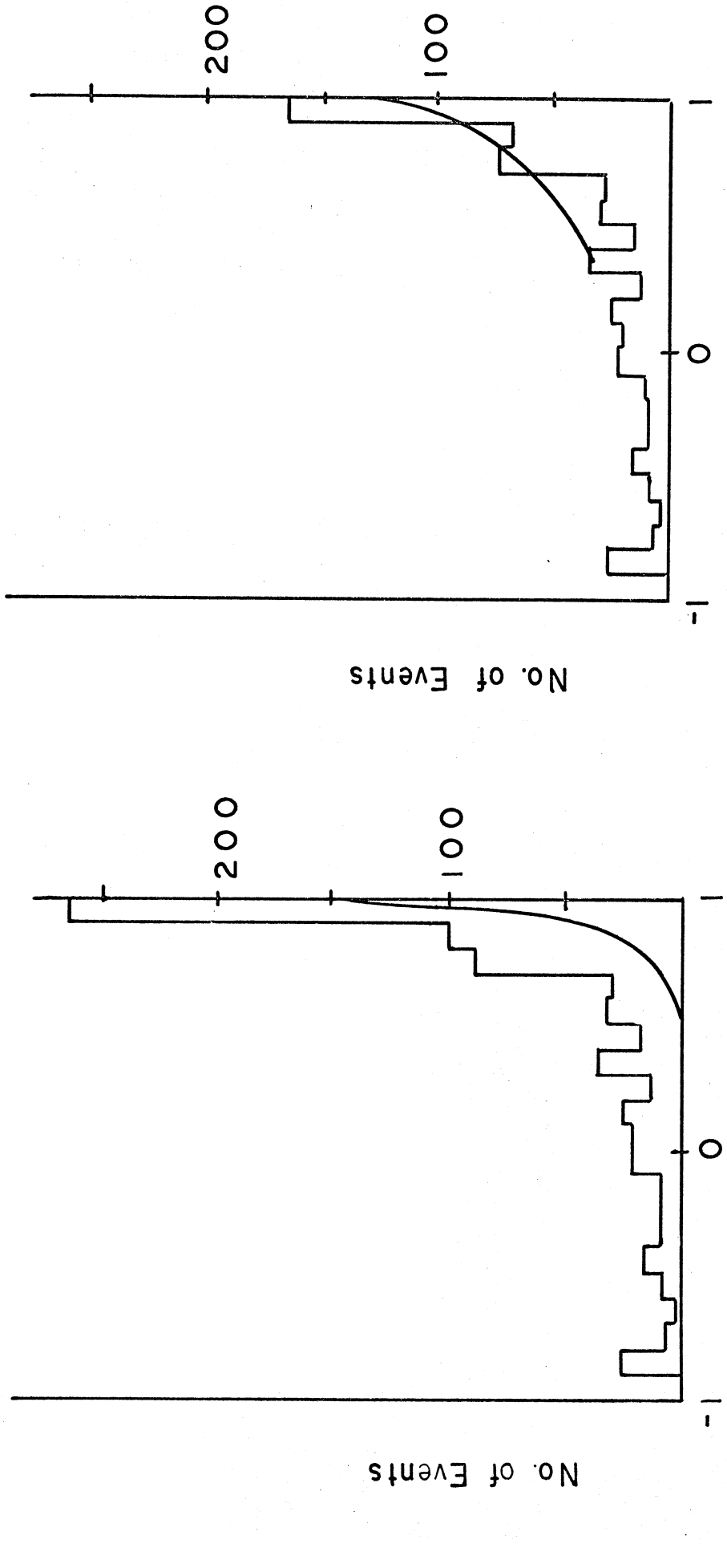

Fig 32.a The scattering angle under the assumption that the proton is initially distributed isotropically with a Hulthén momentum probability.

Fig 32.b The angular distribution of fig 32.a after a background subtraction. The results are compared with n-p elastic scattering.

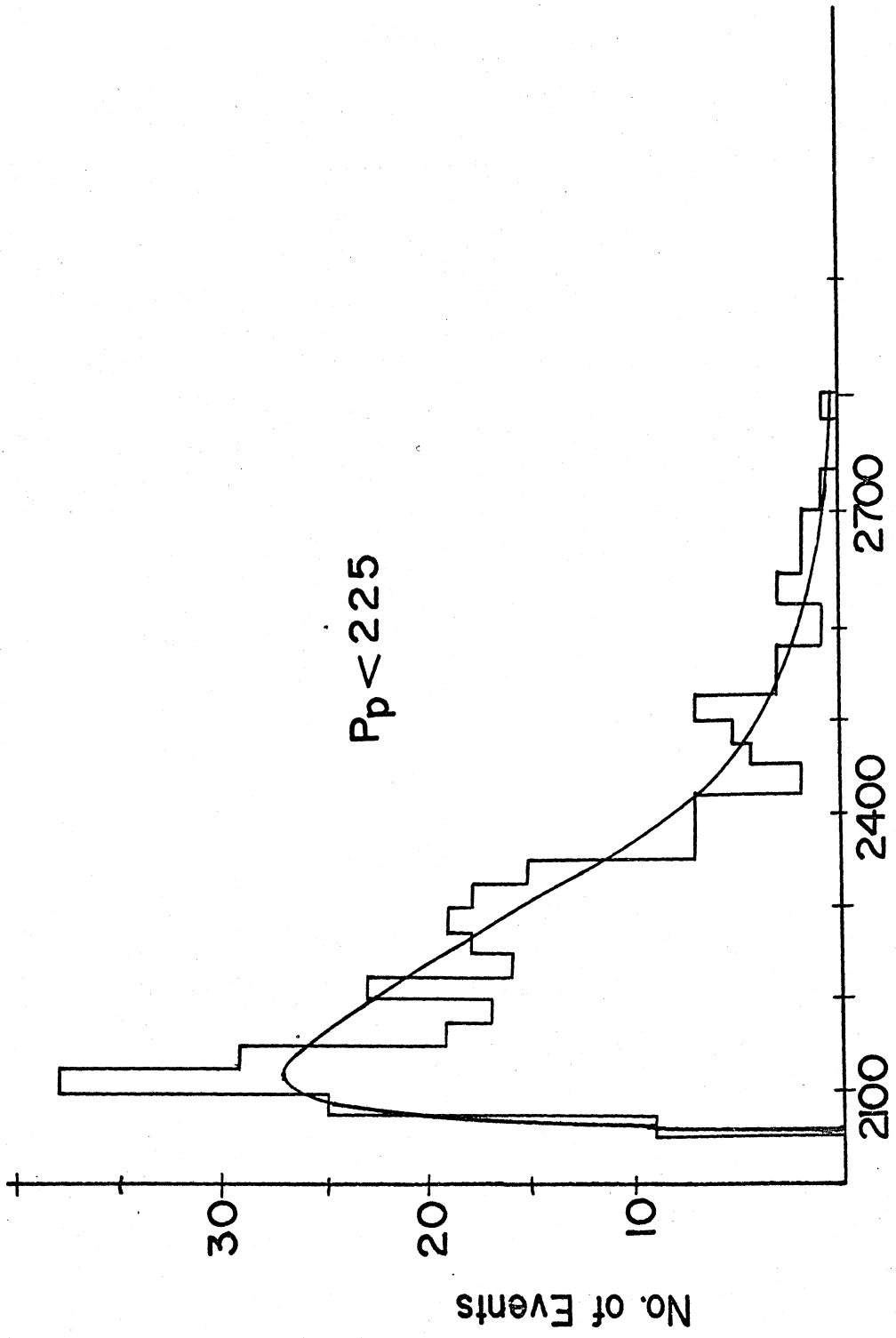

Fig 33. The Λ-P effective mass spectrum of events with $P_P < 225$ Mev/c. For a discussion of the background curve, see text.

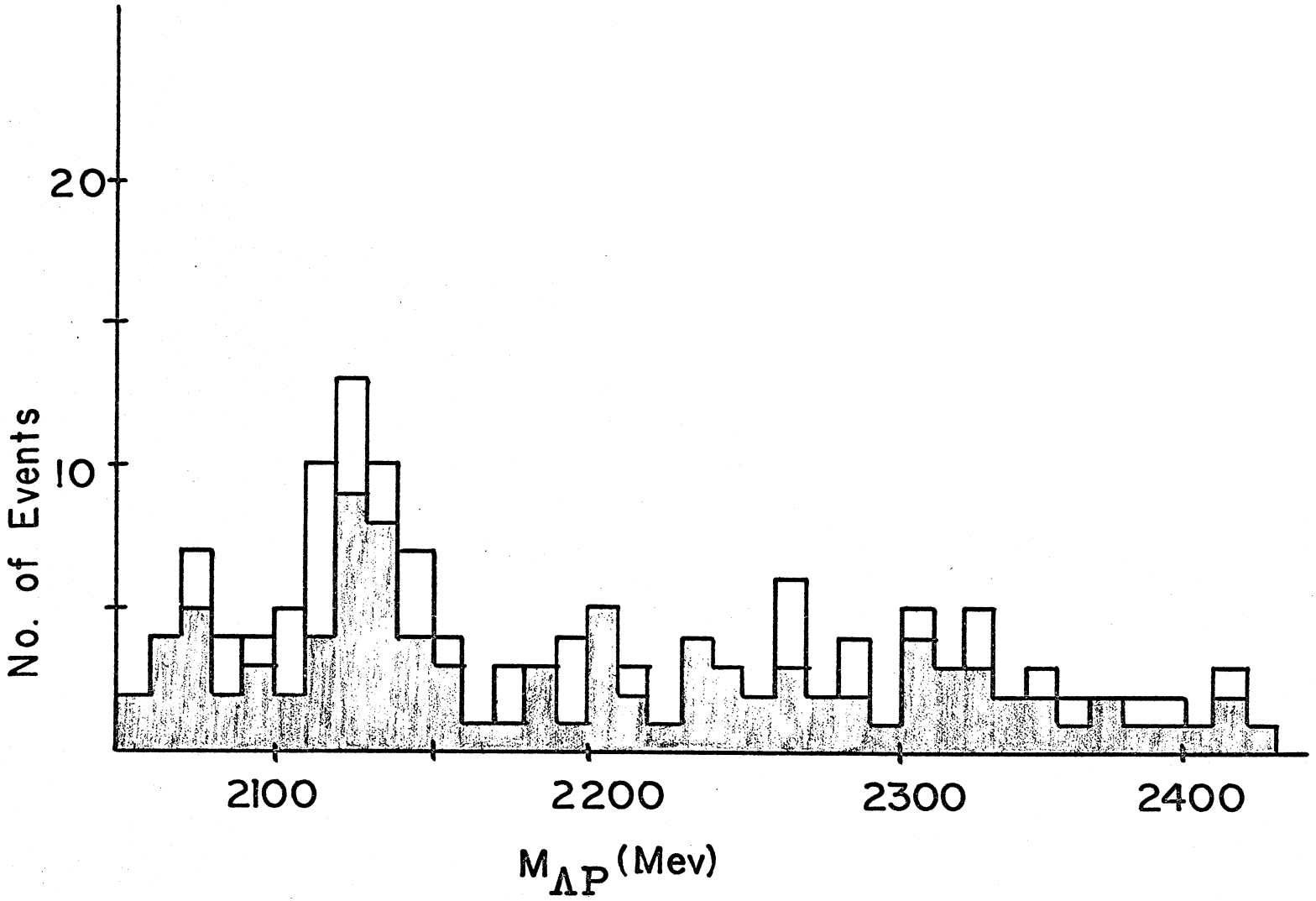

Fig 34. The Λ-P effective mass spectrum of events with $100 < P_p < 225$ Mev/c. The shaded events have $100 < P_p < 150$ Mev/c.

Appendix I:

The Hulthén Theory of the Deuteron

Hulthén describes the static interaction between the proton and the neutron phenomenologically with the potential

$$V(r) = -V_o \frac{e^{-\mu r}}{(1 - e^{-\mu r})} = \frac{-V_o}{e^{\mu r} - 1}$$

where r is the relative distance between the nuclei and V_o and μ are adjustable parameters of the theory, although μ is often taken as the inverse pion compton wavelength

The potential is both central and short range, and for small values of μr since $1 - e^{-\mu r}$ approaches μr

$$V(r) \approx - V_o \frac{e^{-\mu r}}{\mu r} \qquad \mu r \ll 1$$

That is, the Hulthén potential reduces to the Yukawa potential for small μr. However, unlike the case at the Yukawa potential, the resulting Hamiltonian

$$H = \frac{P^2}{2m} - V_o \frac{e^{-\mu r}}{1 - e^{-\mu r}} \qquad m = \frac{Mn\ Mp}{Mn \mp Mp}$$

may be solved by ordinary matrix methods, or the corresponding radial Schroedinger equation

$$\frac{-\hbar^2}{2m} \frac{1}{r^2} \frac{d}{dr} \left(r^2 \frac{d\psi}{dr}\right) - \frac{V_o\, e^{-\mu r}}{1 - e^{-\mu r}} \psi + \ell(\ell+1)\, \hbar^2 \psi$$

$$= E \psi$$

may be solved by making a change of variable.

Setting $\ell = 0$ the resulting wave function is

$$\psi = N \frac{e^{-\alpha r}}{r} (1 - e^{-\mu r})$$

where N is a normalization constant

$$N^2 = \frac{2\alpha (\alpha + \mu) (2\alpha + \mu)}{\mu^2}$$

$$\alpha^2 = \frac{2 |E| m}{\hbar^2}$$

$E = 2.23$ Mev — The binding energy of the deuteron.

$1/\alpha = 4.3 \times 10^{-13}$ cm

The wave function may also be written

$$\psi (r) = N \left(\frac{e^{-\alpha r}}{r} - \frac{e^{-\beta r}}{r}\right)$$

where $\beta = \alpha + \mu$.

The expectation value of the inter-nuclear distance is given by

$$\langle r \rangle = \frac{\int r \left[\frac{e^{-\alpha r}}{r} - \frac{e^{-\beta r}}{r}\right]^2 d\vec{r}}{\int \left[\frac{e^{-\alpha r}}{r} - \frac{e^{-\beta r}}{r}\right]^2 d\vec{r}}$$

This is easily evaluated to yield:

$$\langle r \rangle = \left(\frac{1}{4\alpha^2} - \frac{2}{(\alpha+\beta)^2} + \frac{1}{4\beta^2}\right) \Big/ \left(\frac{1}{2\alpha} - \frac{2}{\alpha+\beta} + \frac{1}{2\beta}\right)$$

choosing $= 7\alpha$ we find

$$< r > = 3 \times 10^{-13} \text{cm}$$

That is to say, the average internuclear separation distance is 3 fermis.

We may estimate the size of the individual nucleons as seen by the incoming pion from pion nucleon scattering cross sections by equating the total cross section to the geometrical cross section πR^2 and solving for R. The π-N cross section in the range 2.6-3.1 Bev is 31.5 mb, from which we obtain a π N radius of about 1 fermi.

Thus, we may crudely picture the deuteron, as seen by an incident pion of momentum 3.65 Bev/c as the dumbell shown in fig. 35 with the separation between the centers of the two parts about 3 fermis, and the radii of each of the ends about 1 fermi.

This "static picture" of the deuteron, however, is misleading since the nuclei oscillates about this mean distance of separation 3 fermis. This may be seen by evaluating the wave function in momentum space

$$\Phi(P) = \frac{1}{(2\pi\hbar)^{3/2}} \int \varphi(r)\, e^{-i \frac{\vec{P}\cdot\vec{r}}{\hbar}}\, d\vec{r}$$

$$= \frac{1}{(2\pi\hbar)^{3/2}} \int N \left(\frac{e^{-\alpha r}}{r} - \frac{e^{-\beta r}}{r}\right) e^{-\frac{iPr}{\hbar}\cos\theta}\, d\vec{r}$$

A straightforward evaluation gives

$$\Phi(P) = N' \left(\frac{1}{\alpha^2 + \frac{P^2}{\hbar^2}} - \frac{1}{\beta^2 + \frac{P^2}{\hbar^2}} \right)$$

where N' is a normalization constant.

Thus, $|\Phi(P)|^2 P^2 dP$ gives the probability that a nucleon will have a momentum in the interval dP about P. The curve $\Phi(P)^2 P^2$ is shown in Figure 36. Note that the curve peaks sharply at about 50 Mev/c, and falls to one-tenth of its peak value at about 225 Mev/c.

The expectation value of r^2 is

$$\langle r^2 \rangle = 2\{ 1/(2\alpha)^3 - 2/(\alpha+\beta)^2 + 1/(2\beta)^2 \}$$
$$\cong 20.44 \text{ f}^2$$

So that the root mean square deviation is

$$\sqrt{\langle r^2 \rangle - \langle r \rangle^2} \approx 3.38\text{f}$$

which gives a measure of the magnitude of the oscillations about the equillibrium position.

Finally, since the time dependence of the wave function of a stationary state is given by[3]

$$e^{-iEt/\hbar}$$

the period of the deuteron oscillation is

$$\tau = \hbar/E = 2.96 \times 10^{-22} \text{ sec.}$$

If the neutron proton bond is broken and one nucleon removed in a period of time short with respect to the period of the deuteron's oscillation, the remaining nucleon will retain its initial momentum in accordance with the "sudden approximation" of quantum mechanics. Thus, if a neutron is struck by an incident projectile and removed from the presence of the proton, the proton will travel a distance of R in a deuterium chamber, where R is given by the range momentum relation

$$R = bp^m$$

with $m = 3.615$

and $b = 1036$

The units of b are such that R is in cm when p is in Bev/c. Whether or not the proton is visible depends on the length of the ionization track as seen by the scanner.

If the scanner looks in the Z direction, he sees a track of length $R\sin\theta$, where θ is the polar angle shown in fig. 37. The probability that this projected length will be greater than Rmin, the shortest visible length, is given by:

$$Pr = \frac{\text{number of ways that } R\sin\theta > Rmin}{\text{number of all possible orientations}}$$

But this quantity is just the ratio of the area between the two hemispherical caps shown in fig. 38 to the total area $4\pi R^2$. That is

$$Pr = \frac{4\pi - 2\int_0^{2\pi} d\varphi \int_0^{\theta = \arcsin(Rmin/R)} d\cos\theta}{4\pi}$$

Evaluating the integral gives

$$Pr = \sqrt{1 - (Rmin/R)^2}$$

In practice, there is not a definite length Rmin below which a track is never seen and above which it is always seen, due to the individual scanner's ability to detect extremely short tracks and due to the statistical nature of bubble formation. A spectator momentum distribution, found by multiplying the above probability in which Rmin = .14 cm, with a Hulthén probability density, was found to agree fairly well with a sample of protons from a different sample of events in the same exposure as ours (Lovell (1967)) for which the protons approximated the behavior of true spectators. This comparison is shown in fig.39.

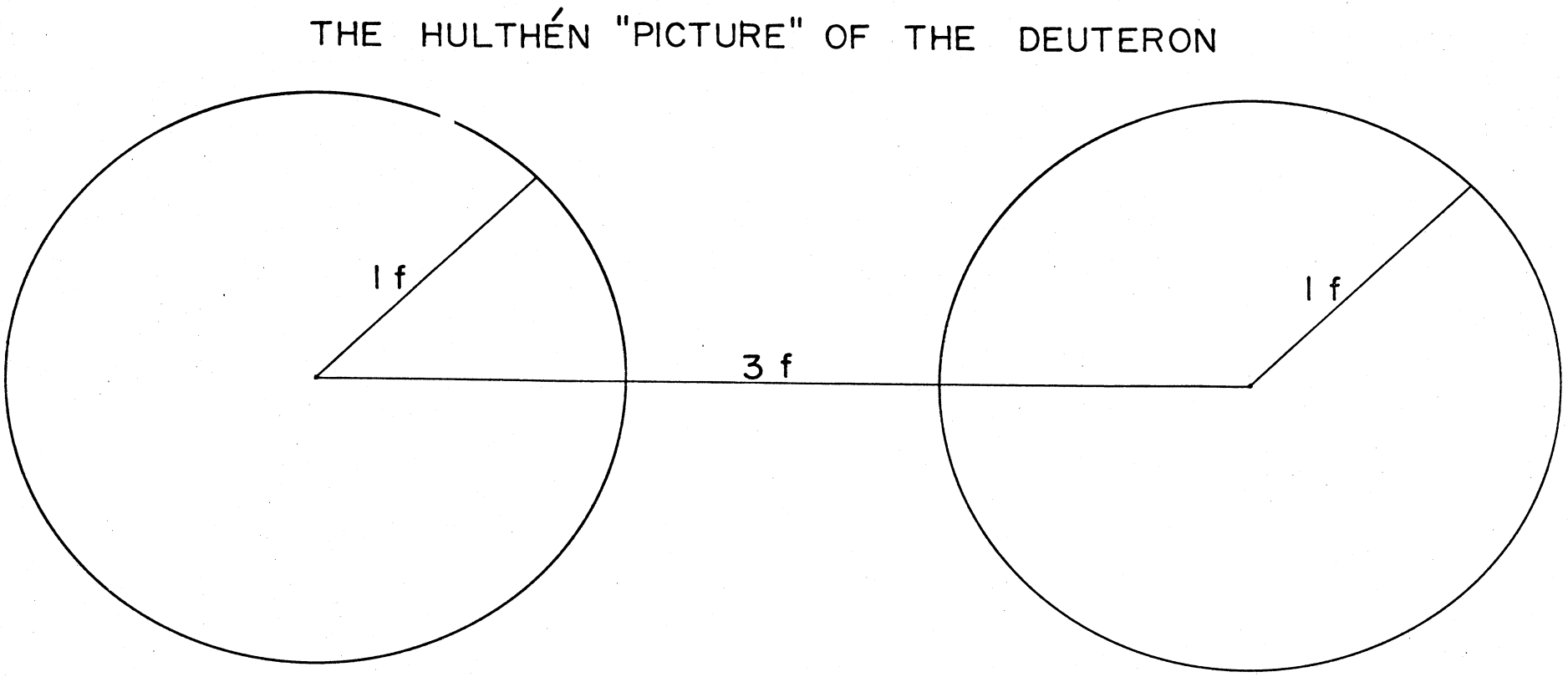

Fig 35. A schematic representation of the deuteron based on the Hulthen theory. (See Text)

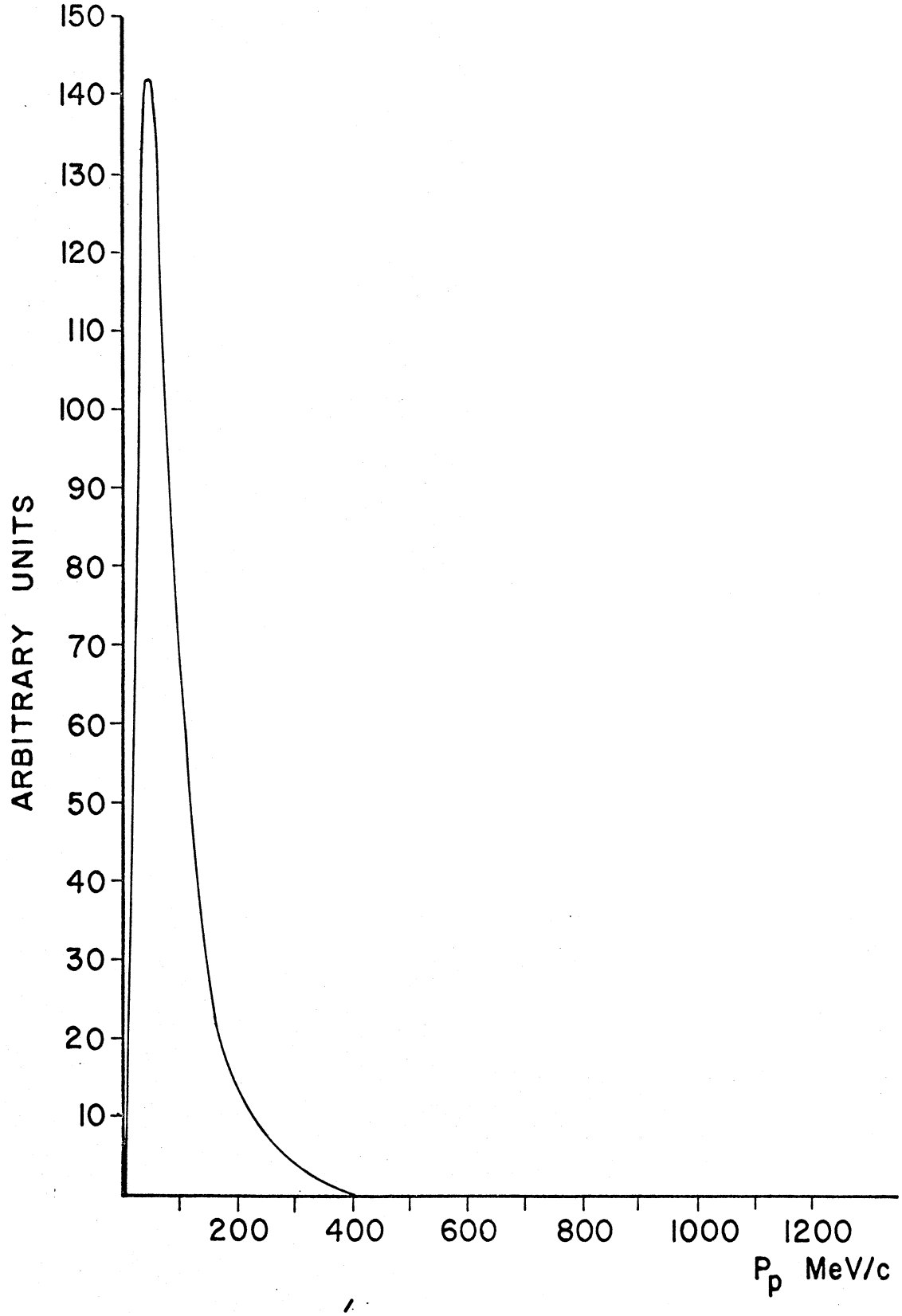

Fig 36. The Hulthén momentum spectrum.

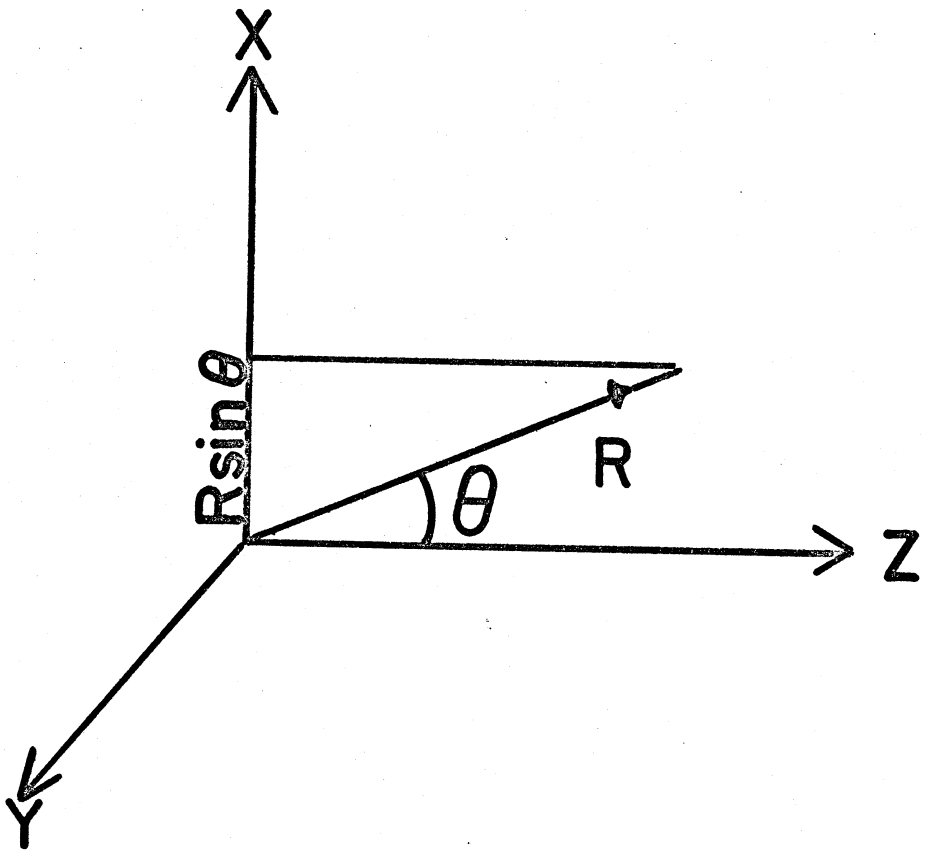

Fig 37. The angle θ defined. (See Text)

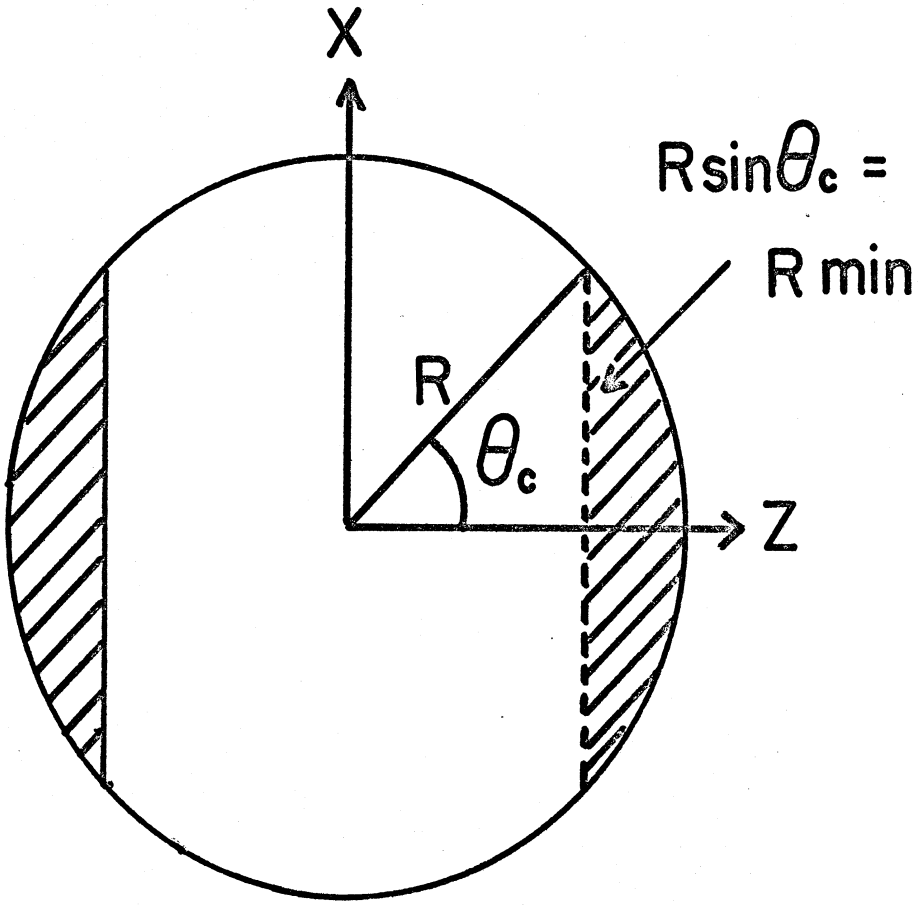

Fig 38. The definition of the limiting angle. (See Text)

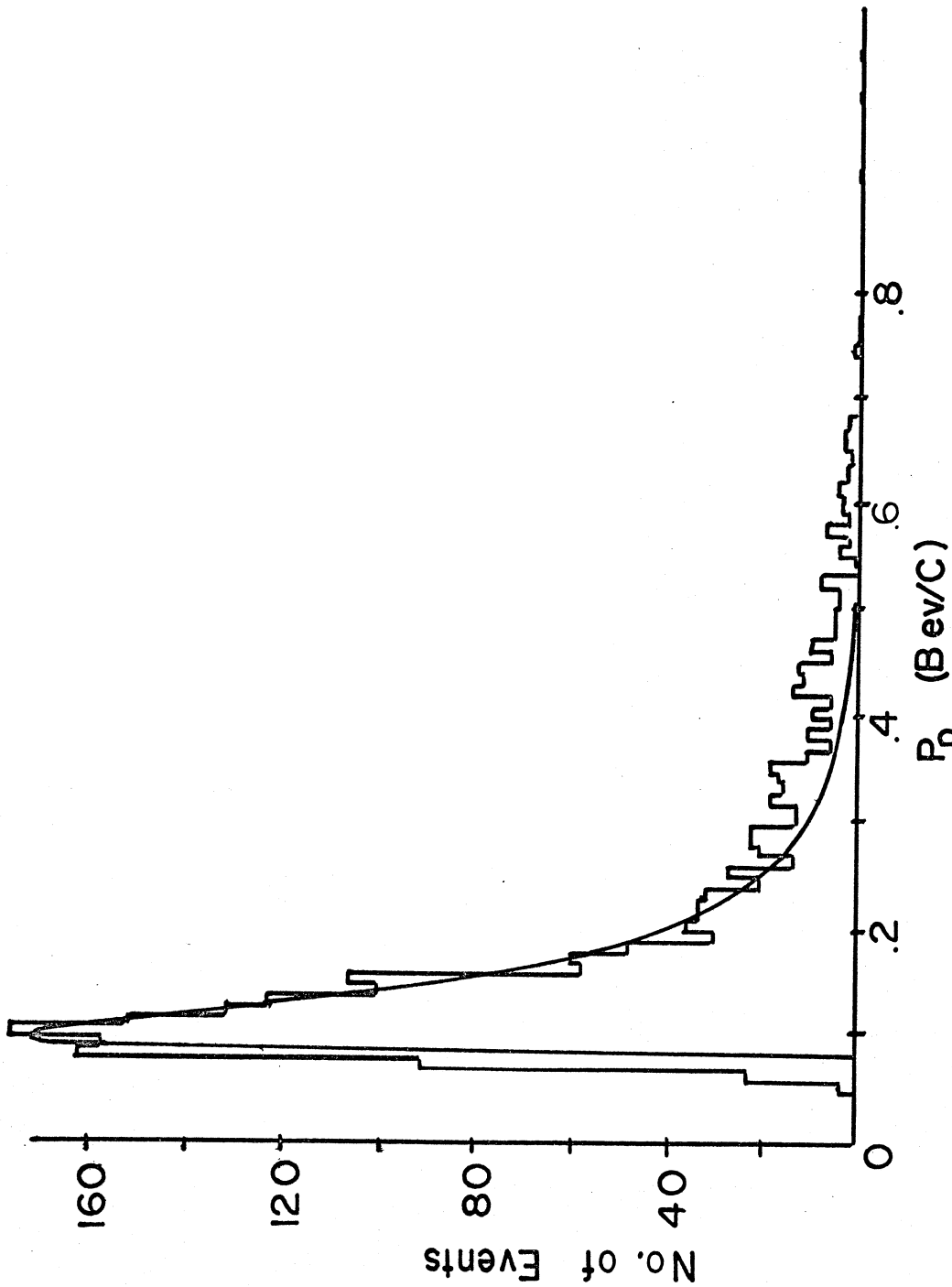

Fig 39. Comparison of the observable spectator distribution with the protons from an earlier experiment. (See Text)

Appendix II

Cusp Phenomena and Σ-Λ Conversions

It is tempting to speculate on the relationship of the enhancement at 2125 Mev to the Σ-P threshold at 2130 Mev. Two types of threshold phenomena may be responsible for an enhancement in the Λ-P effective mass spectrum: a cusp in the Λ-P elastic scattering cross section, and a conversion of Σ's to Λ's upon interacting with a nucleon.

A number of authors have predicted cusp phenomena in Λ-nucleon processes at the Σ threshold. Dullemond and DeSwart(1961,1962) have calculated the Λ-P elastic scattering cross section using phenomenological potentials derived from previous research on the two nucleon problem. The hyperon nucleon system is described by a two component wave function dealing with the Λ-N and Σ-N channels simultaeously:

$$\psi_{YN} = \begin{pmatrix} \psi_{\Lambda N} \\ \psi_{\Sigma N} \end{pmatrix}$$

The potential, then, is a 2 X 2 matrix

$$V = \begin{pmatrix} V_{\Lambda\Lambda} & V_{\Lambda\Sigma} \\ V_{\Sigma\Lambda} & V_{\Sigma\Sigma} \end{pmatrix}$$

where the elements of the matrix depend on the relative distance, the relative angular momentum, and the spin orientations of the two hyperons. Fig. 40 shows the results of their calculation for two sets of nucleon-nucleon potential. In order to more readily com-

pare the predictions of their work with our data, we have multiplied their curves by a "phase space" curve in which the experimentally observed Λ's from events with $p_p < 225$ Mev/c, were folded into Hulthén protons in the momentum range 0-225 Mev/c, so that both visible and invisible protons are included. The results are shown in fig. 41.

It is noteworthy that although a cusp in the Λ-P cross section at the Σ-P threshold is capable of producing a resonance-like peak in our data, the center of the peak is slightly above the Σ-P threshold, whereas the observed value at 2125 Mev is slightly below. This is due to the characteristic rapid rise of the cross section just below the cusp, and its relatively slow decline above, as exemplified in fig. 40.

It is possible that the hyperon produced in the π-N collision is not a Λ, but a Σ which subsequently converts to a Λ. This is depicted schmatically in fig. 43. The propensity of Σ's to convert to Λ's in the presence of other nucleons is well known. Webb et al (1958) found that for K^- absorbtion stars in nuclear emulsions, 58% of the hyperons converted to Λ's. Dahl et al (1961) found that the process $\Sigma\ N \rightarrow \Lambda\ P$ was important in the reaction $K^-\ D \rightarrow \Lambda\ \pi^-\ P$. Little is known about the angular distribution of such conversions, although the theoretical work of Dullemond and DeSwart (1961) predicts a low energy conversion angular dis-

tribution peaked in the foreward direction for the process $\Sigma^+ n \rightarrow \Lambda P$.

As pointed out by Karplus and Rodberg (1959), moreover, the conversion may occur below the Σ-N threshold. This follows from the fact that the Σ need only travel on the average 3 fermis before interacting and hence, on the basis of the uncertainty principle, may be as much as 65 Mev off the mass shell. Karplus and Rodberg (1959) have derived Σ-Λ conversion amplitudes for the process $\Sigma N \rightarrow \Lambda N$. They find that the Σ Λ conversion probability is of the form:

$$Pr_{\Sigma P \rightarrow \Lambda P} = \frac{k\eta}{(1-ka)^2+(k\eta)^2} \qquad M_{\Lambda P} < 2130 \text{ Mev}$$

$$= \frac{k\eta}{(1+ka)^2+(k\eta)^2} \qquad M_{\Lambda P} > 2130 \text{ Mev}$$

where k is the relative momentum and η and a are parameters. In a certain range of these parameters there is a peaking in the conversion probability slightly below the Σ-P threshold. Fig. 42 shows the conversion probability, as a function of $M_{\Lambda P}$, for some representative values of the parameters in this range. The theory admits a bound state in the Σ-N system which quickly decays into the Λ-P system with a binding energy given by

$$E_B \cong 1/(2\mu_{\Sigma N})(1/a)^2$$

where

$$\mu_{\Sigma N} = \frac{M_\Sigma M_N}{M_\Sigma + M_N}$$

For a $\approx$ .005 $(\text{Mev/c})^{-1}$, the binding energy is $\sim$20 Mev.

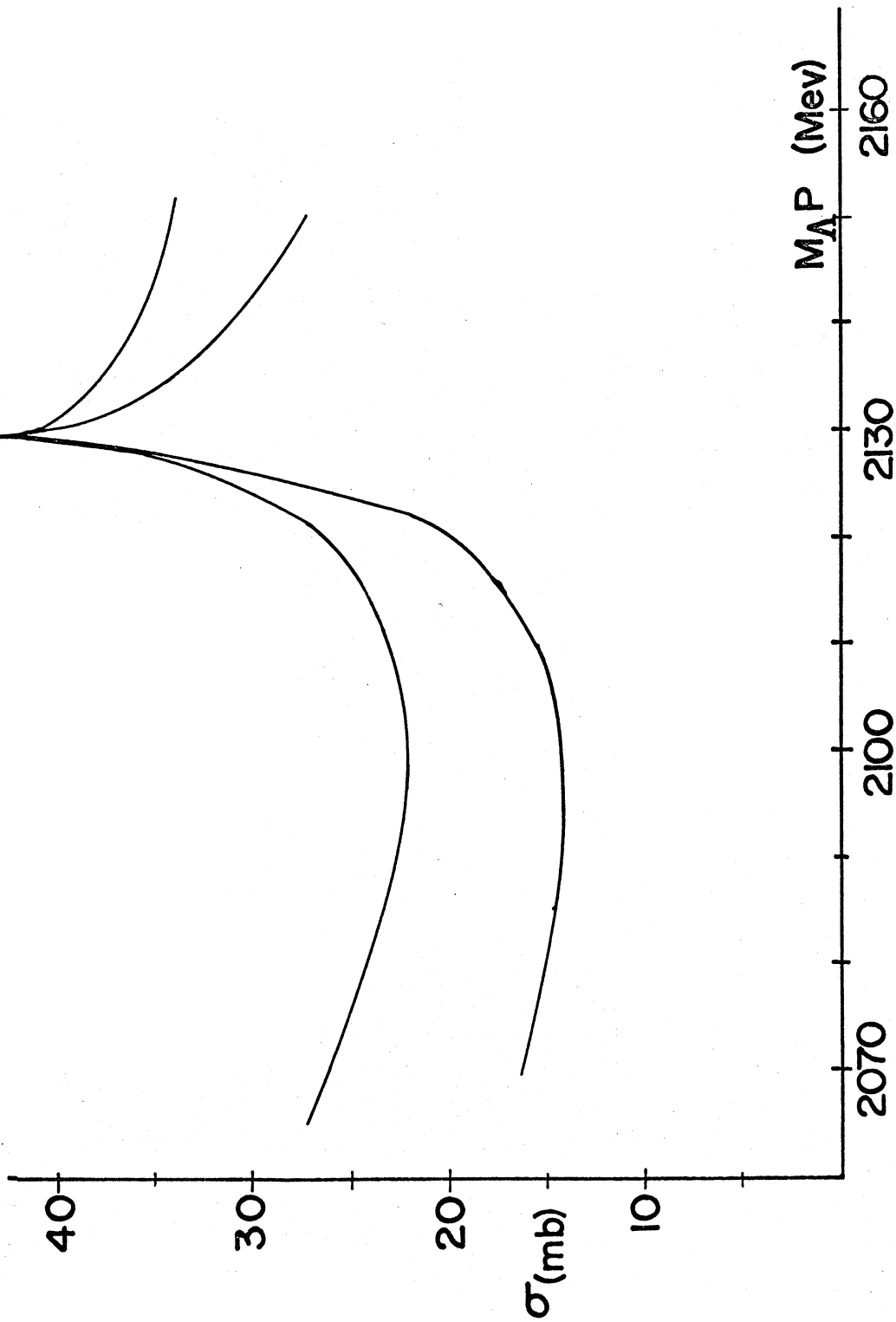

Fig 40. The Λ-P elastic scattering cross section near the ΣN threshold as predicted by Dullemond and De Swart (1962). The two curves result from different choices of the potential energy.

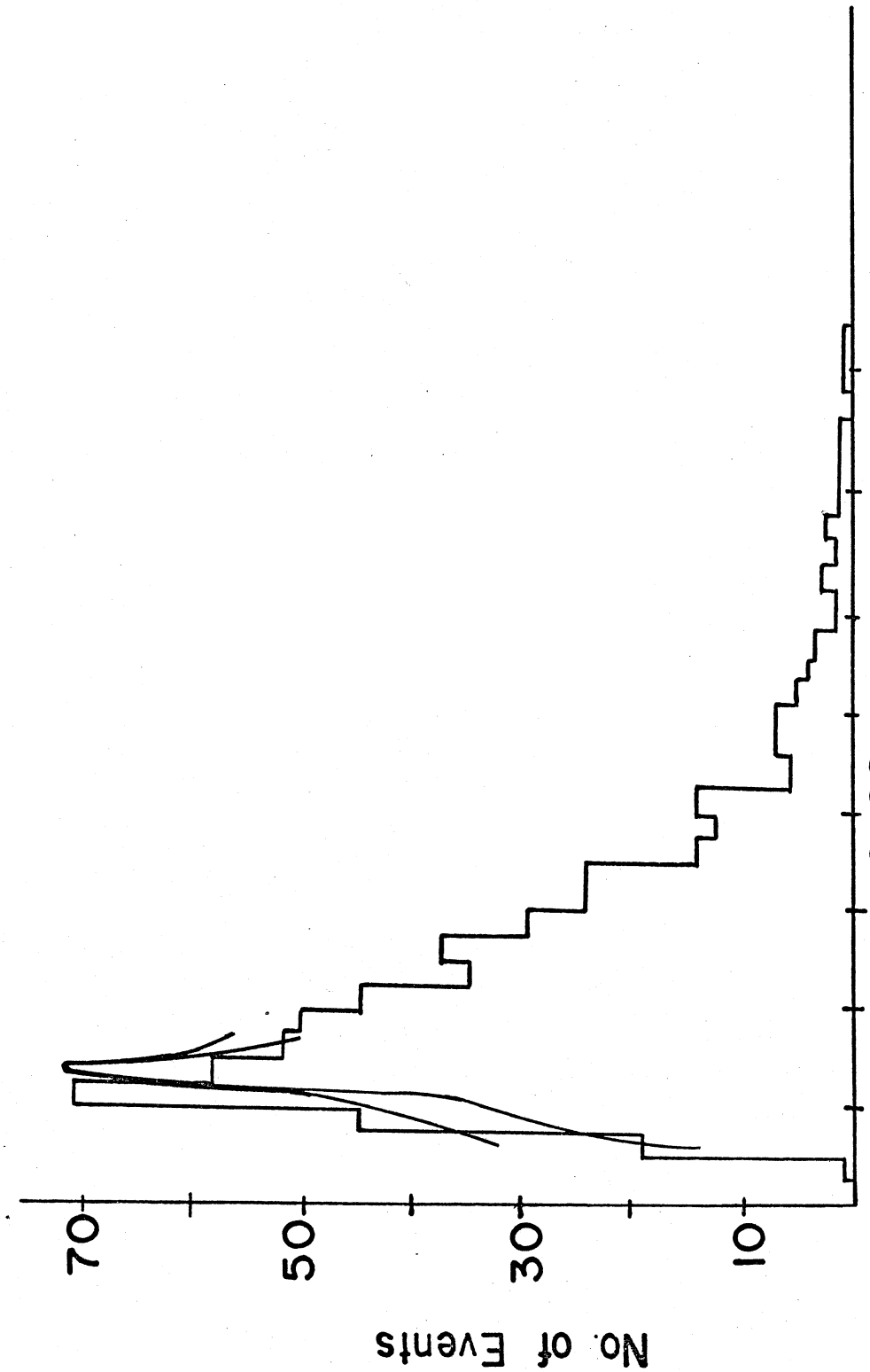

Fig 41. A comparison of the predictions of Dullemond and De Swart (1962) with our data. (See Text)

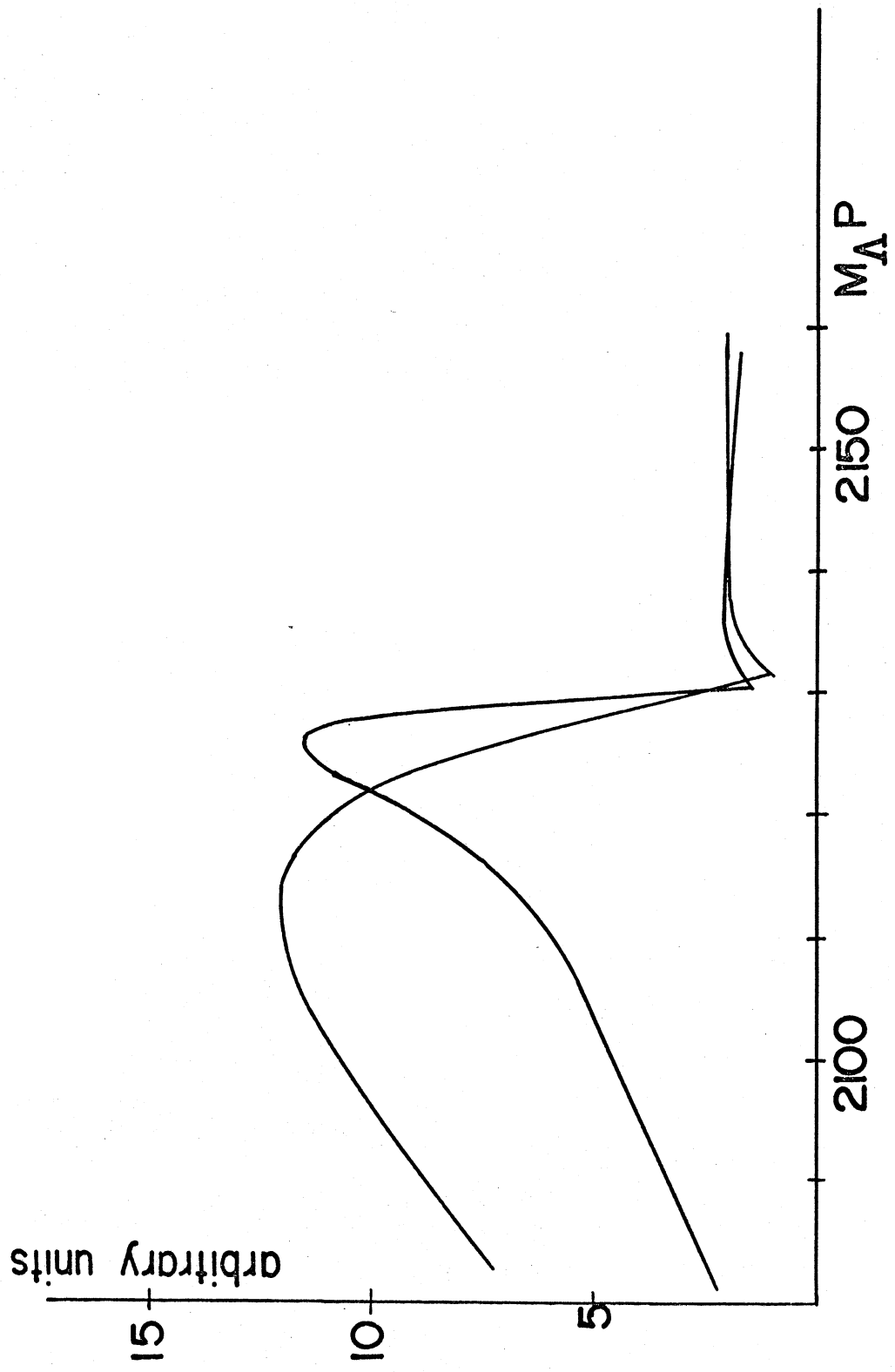

Fig 42. The $\Sigma \rightarrow \Lambda$ conversion probability of Karplus and Rodberg (1959) for certain values of their parameters.

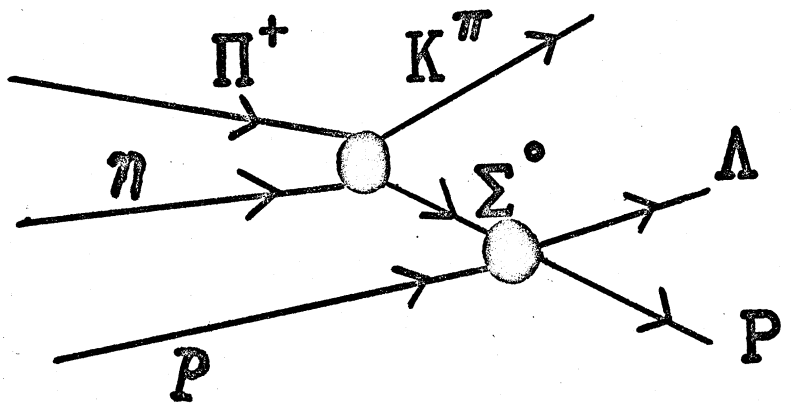

a.

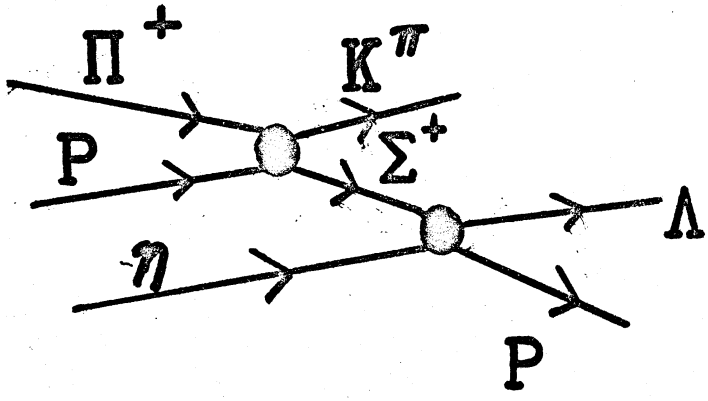

b.

Fig 43. A schematic representation of intermediate Σ states.

REFERENCES

G. Alexander, J. Anderson, F. Crawford, W. Lasker, and L. Lloyd, Phys. Rev. Letters 7, 348 (1961)

G. Alexander, U. Karshon, A. Shapira, G. Yekutieli, R. Englemann, H. Filthuth, A. Fridman, and A. Minguzzi, Phys. Rev. Letters 13, 484 (1964).

G. Alexander, O. Benary, U. Karshon, A. Shapira, G. Yekutieli, R. Englemann, H. Filthuth, A. Fridman and B. Schiby, Phys. Letters 19 715 (1966)

S. Ali, M. E. Grypeos and L. P. Kok, Phys. Letters 24B 543 (1967).

B. A. Arbuzov, E N. Kladnitskaya, V N. Penev, and R. N. Faustov, JETP 42, 979 (1962), Soviet Phys. JETP 15, 676 (1962).

D. Bassano, C. Chang, M. Goldberg, T Kokuchi, and J. Leitner, Phys. Rev. 160, 1239 (1967)

P. Beilliere, J. L. Gomez, A. Lloret, A. Rousset, K. Myklebost, and J. M. Olsen, Phys. Letters 12, 350 (1964).

G. Benson, Mesons and Spectator Protons in $\pi + d \rightarrow \pi^+\pi^-\pi^o$ pp at 3.65 Bev/c, University of Michigan technical report coo. 11/2-4. (1966)

T. Buran, O. Eivindson, O. Skjeggestad, H. Tofte and I. Vegge, Physics Letters 20 318 (1966).

G. Chew and G. Wick, Phys. Rev. 85, 636 (1952)

D. Cline, R. March, M. Sheaff, Phys. Letters 25 466 (1967).

H. O. Cohn and K. H. Bhatt, Phys. Rev. Letters 13 668 (1964).

F. S. Crawford, M. Cresti, M. L. Good, F. T. Solmitz, M. L. Stevenson, and H. K Ticho, Phys. Rev. Letters 2, 174 (1959)

O. Dahl, N. Horwitz, D. Miller, J. Murray, P. White, Phys. Rev. Letters 6, 142 (1961).

J. J. DeSwart and C. Dullemond Ann. Phys., 16, 263 (1961).

J. J. DeSwart and C. Dullemond, Nouvo Cimento, 25, M.5, 1072 (1962)

T. H. Groves, Phys. Rev. 129, 1372 (1963).

W. Hess, Rev. Mod. Physics, 30, 368 (1958)

L. Hulthén and M. Sugawara, Handbuch der Physik (Springer-Verlag, Berlin, 1957), Vol. 39, p. 1.

R. Karplus, L. Rodberg, Phy . Rev. 115 1058 (1959)

T. Kotani and M. Ross, Nuovo Cimento 14, 1282 (1959)

L. Lovell, Private Communication (1967)

A. C. Melissinos, N. W. Reay, J. T. Reed, T. Yamanouchi, E. Sacharidis, S. J. Lindenbaum, S. Ozaki and L. C. L. Yuan, Phys. Rev. Letters 14 604 (1965).

W. Moebs, University of Michigan technical report COO - 11/12 - 3 (1965).

L. Piekenbrock and F. Oppenheimer, Phys. Rev. Letters 12, 625 (1964).

P. A. Piroue, Physics Letters 11 164 (1964).

A. Rosenfeld, N. Barish-S hmidt, A. B rbaro-Galtieri, W. Podolsky, L. Price, P. Soding, C. Wohl, M. Roos, and W. Willis, Lawrence Radiation Laboratory Report UCRL-8030 (1967).

B. Sechi-Zorn, R. A. Burnstein, T. B. Day, B. Kehoe, and G. A. Snow, Phys. Rev. Letters 13, 282 (1964).

V. F. Vishnevskii, Tu Yuan-Ch'ai, V. I. Moroz, A. V. Nikitin, Yu. A. Troyan, Chien Shao-chun, Chang Wen-yu, B. A. Shakhbazyan, and Yen Wu-kuang, Soviet Journal of Nuclear Physics 3 511 (1966).

T. Wangler, University of Wisconsin Thesis (1964).

T. Wangler, Private Communication (1966). I would like to thank Drs. A. Erwin and W. Walker for making Wangler's data available to me.

F. Webb, E. Iloff, F. Featherson, W. Chupp, G. Goldhaber, and S. Goldhaber, Nuovo Cimento 8, 899 (1958).

ACKNOWLEDGEMENTS

It is a pleasure to acknowledge the help of the following people, to all of whom I am deeply grateful:

Dr. John Vander Velde for serving as chairman of my doctoral committee, as well as for his patient guidance throughout the experiment,

Dr. T. Murphy for the interest shown in the progress of the experiment,

Drs. M. Ross, R. Lewis, and F. Shure for serving as doctoral committee members,

our technical staff, particularly D. Moebs, V. French, M. Rauer, and A. Loceff,

my fellow graduate students for assistance and many interesting discussions; in particular, the late G. Benson, L. Lovell, A. Fisher, D. Falconer, M. Church, and C. Arnold,

G. Kane and M. Ross for helpful discussions,

J. Besancon and N. Higbee for drafting most of the figures in this report,

K. Herholtz and D. Shoemaker for typing the draft,

The Bubble Chamber Group, under Dr. Daniel Sinclair, for financial support throughout the duration of the experiment.